Zeitschrift Kunststofftechnik
Journal of Plastics Technology

www.kunststofftech.com · www.plasticseng.com

archivierte, peer-rezensierte Internetzeitschrift
archival, peer-reviewed online Journal

WAK Wissenschaftlicher Arbeitskreis Kunststofftechnik
Scientific Alliance of Polymer Technology

eingereicht/handed in: 05.07.2022
angenommen/accepted: 06.02.2023

Dominik Boos[1], Tim Scherzer[2], Kalle Kind[1], Swen Zaremba[1], Klaus Drechsler[1]
[1]Chair of Carbon Composites, Technical University of Munich
[2]Department of Polymer Engineering, University of Bayreuth

Towards a Robust, Water-Soluble, Lost Core Material – part one: Unreinforced, Binder-Free Salt

Hollow constructions save emissions through a high material efficiency. However, this results in complex geometries, which can only be realized with expendable or so-called "lost" cores. This study focuses on the salt core technology, which has been rather disregarded in plastics technology so far. It is investigated how water-soluble salt cores can be implemented in the composite process routes injection molding and automated fiber placement (AFP). Different process experiments with commercial salt cores show the potential and challenges that arise. This paper deals with binder-free, non-reinforced salt cores that are state of the art in light metal casting. In a follow-up paper, fiber-reinforced salt cores will be introduced that exhibit a higher processing stability.

Entwicklung in Richtung eines robusten, wasserlöslichen, verlorenen Kernmaterials – Teil 1: Unverstärktes, binderfreies Salz

Durch Hohlbauweise wird eine hohe Werkstoffeffizienz erreicht, was Emissionen einspart. Jedoch entstehen dadurch komplexe Geometrien, die sich in Kombination mit anspruchsvollen Prozessrandbedingungen nur mit verlorenen Kernen umsetzen lassen. Daher behandelt diese Studie die in der Kunststofftechnik bislang weitgehend ungenutzte Salzkerntechnologie. Es wird untersucht, wie wasserlösliche Salzkerne in den Composite-Prozessen Spritzguss und automatisiertem Tapelegen eingesetzt werden können. Verschiedene Prozessexperimente mit kommerziellen Salzkernen offenbaren das Potential und die Herausforderungen. Dieser Artikel behandelt unverstärkte Salzkerne ohne Binder, welche Stand der Technik im Leichtmetallguss sind. In einem nachfolgenden Beitrag werden faserverstärkte Salzkerne mit einer höheren Prozessstabilität vorgestellt.

Towards a Robust, Water-Soluble, Lost Core Material – part one: Unreinforced, Binder-Free Salt

D. Boos, T. Scherzer, K. Kind, S. Zaremba, K. Drechsler

1 WATER-SOLUBLE SALT AS AN EXPENDABLE TOOLING MATERIAL

1.1 State of the Art

The parts of a tool that are used up during a production process (e.g. casting) and then no longer have their original shape or structure are referred to as expendable cores, lost cores, or semi-permanent mold. They initially remain on the produced component after the forming step and are removed in a separate process step. Restrictions regarding demolding like draft angles or undercuts may be ignored. This grants the designer a high degree of freedom to achieve the optimal functional geometry. With this concept, a consistent, lightweight and cost-efficient integral design can be pursued. Avoiding differential design saves subsequent processes such as assembly, sealing, welding, machining or complicated core pulling mechanisms [1–3]. Competitive methods like gas- or water-assisted injection technology cannot produce precise inner contours for different wall thicknesses [4, 5], which are, for instance, important for media flow efficiency.

Another application of such mold materials is the in-situ assembly or embedding of entire assemblies (e.g. gear set in gearbox housing) [3, 6]. In this case, the mold material does not only define the geometry, but also serves as a protection for the wrapped or filled parts in subsequent process steps until it is removed and the assembly can be put in service [3, 6].

Especially fiber-reinforced plastics can benefit from the great design freedom that is enabled by robust lost cores. The combination of hollow sections or undercuts and tailored anisotropy, that can be achieved with an individual fiber stacking, exploits the maximum lightweight potential of a structure. Thus, fiber composites can outperform conventional metal constructions.

In the injection molding industry, fusible cores based on low-melt alloys are used as lost cores to build up complex shaped parts with flow channels that require a high surface quality and contour accuracy. The low-melt alloy melting point should be below the polymer melting point [1]. Undesired melting of the core during the plastic injection is prevented by a minimum wall thickness of the core and its better heat conductance compared to the polymer [1, 3]. Usually, glass fiber-reinforced polyamide is injected over a tin-bismuth core for typical

applications like inlet manifolds or pump casings for the automotive industry [3, 7, 8]. Furthermore, there are CF-PEEK aircraft parts that were injection molded with a fusible core [9, 10]. However, the demonstrator part showed the limits of the technology, because the core needed an extra water cooling during injection in order to keep the tolerance specifications [9]. In general, low-melt alloys have some disadvantages that might prevent its breakthrough in the plastics industry. The high cost for the raw materials and plants primarily limit its efficiency to a series production [3, 11]. The high density and environmental aspects make them difficult to handle during processing and disposal. A possibly remaining metal film contaminates the surface and increases the weight of the plastic part. Another problem might be the exposition of parts to high temperatures during melting out of the core material that can change the molecular structure of the plastic.

Water-soluble salt does not suffer from these drawbacks, but it seems like it has not gotten much attention in the plastics industry so far. Little information can be found in literature [3] about its application in injection molding and the results did not encourage further research due to its lack of strength. However, a patent reports on successful overmolding attempts with PS and PP [12]. In addition, water-soluble salt cores are occasionally used in resin transfer molding (RTM) [13, 14] and winding [15] process routes for FRP parts. Xiao [13] designs a binder-stabilized NaCl core for a cavity in an CFRP omega-stiffener. The salt core achieves a compressive strength of 57.3 MPa and a flexural strength of 10.2 MPa that enabled a successful processing in RTM and core removal. A similar salt material is investigated for a T-joint part in ABS injection molding by Lin [16]. The binder-stabilized salt was completely encapsulated in two plastic shells to protect the core and the core prevents the collapse of the shells respectively. Thiede-Smet [14] mentions low-melting eutectic salts with melt temperatures up to 270 °C as a possible material for RTM without giving specific strength values or application examples. Keller [15] uses a low-melting eutectic salt, namely Paraplast 36 (from Resolin Inc., Chatsworth, California) as mandrel for wet filament winding. Its bending strength was not reported. It has to be noted, that the mechanical properties of the above-mentioned salts materials [13–15] may be sufficient for the application they were designed for, but will probably show bad performance in injection molding due to their poor flexural strength and temperature stability. Therefore, binder-free salts and salt mixtures with higher melting points are more appropriate for higher process loads. Such salts are already intensively used in light metal casting for special undercut geometries (e.g. closed deck cylinder blocks, piston cooling channels), because they offer a better strength and surface quality than binder-stabilized sand or salt cores [17–21]. Among the casting techniques, the high-pressure die casting (HPDC) is the most economically effective process to produce complex, near-net shape 3D parts in a large volume with a low wall thickness and thus offering a high lightweight potential [17, 22–28].

Aluminum HPDC benefits from the technology spectrum in the automotive industry ranging from combustion engines to electric powertrains and hybrid vehicles. For a successful switch to the e-mobility and a higher efficiency, there

will be a growing demand for more complex and hollow light metal parts [22, 24, 25, 29–31]. Aluminum HPDC parts are prone to welding defects, i.e. ensuring weldability needs much effort [28, 32], which is why a single part design should be preferred.

The HPDC process is similar to injection molding, however, the parameters are different, due to the differing melt characteristics. Typical HPDC conditions for aluminum alloys are: 30 to 60 m/s gate velocity, 1200 bar packing pressure [33], mold temperatures between 120 °C and 280 °C in combination with melt temperatures up to 700 °C [34] depending on the alloy and cavity design. The fill times usually range from 10 ms to 150 ms [34] and machine cycles last from seconds to several minutes [35]. The loads on a lost core are comparable with injection molding.

In the past, there has been intensive research on salt cores, mostly for a HPDC application. There are three production methods: sintering (S) of a powder or slurry, casting of a melt and wet compression molding (WCM) of a slurry. The sintering and WCM process sequences are similar. Both start with a powder, which has a defined grain size spectrum or median particle diameter. To achieve the desired rheological and thermodynamic properties dry or liquid additives are added prior to sintering. A green body is then produced under a high consolidation pressure (p_c) in a press (P) or heated press (HP). Higher temperatures in the compression phase may start sinter mechanisms or drying of the green body. After that, it is usually sintered in an oven at sinter temperature (T_{sinter}) for a certain dwell time to achieve the final strength. In case of WCM the sintering is not necessary, because the water enables material transport mechanisms at low temperatures [22]. A process variant without a press can be an additive process with a dropwise material deposition [36]. The casting techniques can be further divided in gravity casting (GC), low-pressure die casting (LPDC) and HPDC. In the beginning, different salt species are mixed to obtain a hyper- or hypoeutectic composite salt. It is molten in a crucible slightly above melt temperature up to the casting temperature (T_{cast}) and then poured into a mold that is preheated to the mold temperature (T_{mold}). In case of LPDC and HPDC, a piston pushes the salt melt from the shot sleeve into the mold. Compression molding [13] and injection molding or shooting [37–39] methods for binder-stabilized salt cores also exist, but they will not be discussed further in this article, because of the low strength and high porosity of cores produced in such ways. For the same reason, other water-soluble core materials based on binders, for example CavusCore [40], are excluded here. Table 1 provides an overview of the state of art in processes and materials with the most important parameters. Figure 1 depicts the corresponding bending strengths if any are given.

Process	Material	T_{cast} or p_c	T_{mold} or T_{sinter}	Source
GC	NaCl-Na_2CO_3 hypereutectic	763 °C	100 °C	Yaokawa 2007 [20]
HPDC	Na_2CO_3-NaCl-KCl	n. a.	250 °C	Oikawa 2009 [41]
P	NaCl powder (5 µm)	*165 MPa*	n. a.	Fuchs 2014 [22]
WCM	NaCl powder (26 µm) + water	*165 MPa*	*35 - 125 °C*	Fuchs 2014 [22]
GC, HPDC	NaCl-$NaCO_3$ hypoeutectic	680 °C	200 °C	Fickel 2014 [24]
HPDC	KCl-Na_2CO_3	n. a.	n. a.	Pierri 2016 [42]
HPDC	NaCl-Na_2CO_3-KCl	liquidus + 20 °C	250 - 350 °C	Kallien 2016 [23], 2014 [43], 2013 [44]
GC	Mixture based on KCl	400 - 500 °C	125 - 150 °C	Huang 2017 [45]
HP + S	NaCl powder + additives	*60 - 200 MPa*	*650 - 730 °C*	Hartig 2018 [18], Grözinger 2011 [46], 2005 [47]
GC	NaCl-Na_2CO_3 ($6CO_3$-series)	710 °C	100 °C	Oikawa 2018 [48]
P + S	NaCl powder (0.35 mm)	*235 MPa*	*600 °C*	Vitor 2018 [49]
GC	KCl-KNO_3 + bauxite/ sericite powder	liquidus + 15 °C	130 - 160 °C	Tu 2018 [50]
LPDC	n. a.	n. a.	n. a.	Findeisen 2019 [51]
GC	KCl-KNO_3 + 12.5 µm glass fiber	485 °C	180 °C	Gong 2020 [52]
GC	KCl-K_2CO_3	850 °C	200 °C	Cantas 2020 [53]
GC	KCl-KNO_3 + bauxite powder + glass fibers < 75 µm	455 °C	140 - 160 °C	Liu 2020 [54]
LEF + S	Na_2SO_4 + NaCl + bauxite powder (12.5 - 75 µm) + ethanol	n. a.	*630 °C*	Gong 2021 [36] (preprint)
GC	NaCl-Na_2SO_4	800 °C	300 °C	Wang 2022 [55]

Table 1: Overview of salt cores without binders. If there are several material or process variants, just the one with the highest strength is shown. Salt powder specifications are complemented by the median particle diameter. P: press process, HP: hot press process, S: sinter process, LEF: layered extrusion forming, GC: gravity casting, HPDC: high-pressure die casting, LPDC: low-pressure die casting, WCM: wet compression molding, p_c: consolidation pressure, T: temperature

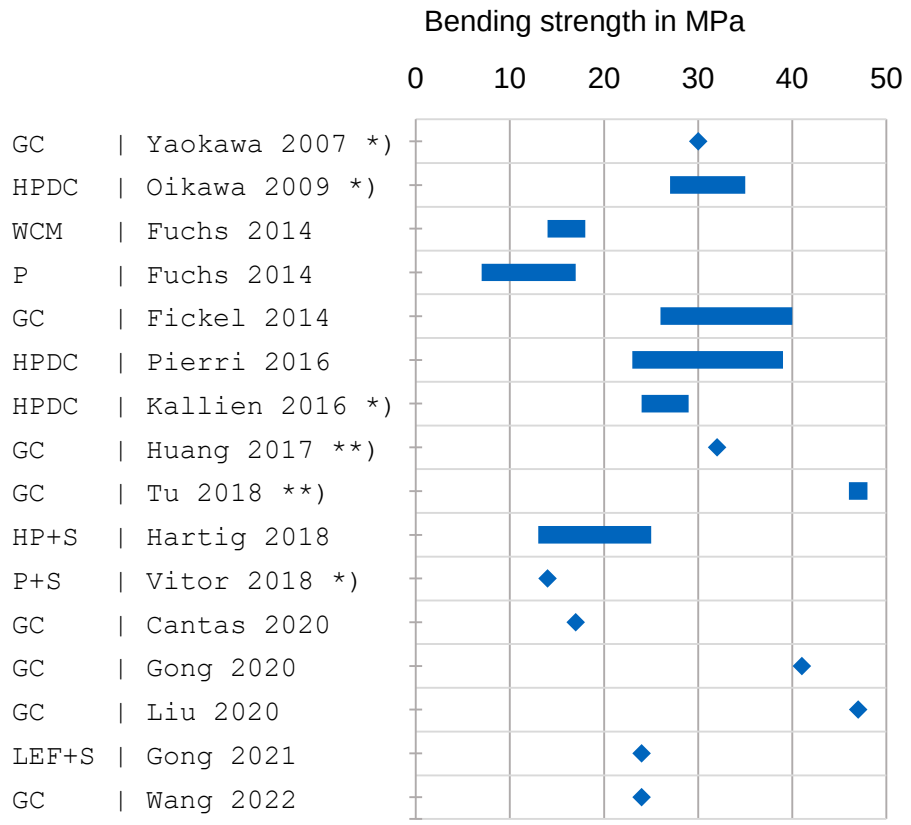

*Figure 1: Overview of reported three-point bending test strength values in literature listed in Table 1. If there were several material or process variants, just the one with the highest strength is shown. The strength range (bar) or highest strength value (diamond) is presented depending on the available data. Please note, that the diagram shows three-point bending test results except for: *) four-point bending test and **) bending test not specified.*

Every production method has its benefits and drawbacks. The compression molding methods require high consolidation pressures that limit the part size and complexity [37]. The raw material - the salt powder - must have a defined grain size spectrum [22]. Otherwise, the sintering might not lead to the optimal density and strength [56, 57]. Furthermore, in case of uniaxial pressing, the microstructure might suffer from density gradients that occur from friction effects for high wall thickness in compaction direction and high press forces [58, 59]. For example, a sintered salt core with more than 50 mm height has density gradients up to 20% which result in deformation, cracks or fracture during HPDC [26]. In this aspect, the wet compression method is more tolerant, because the water acts as a temporary lubricant that leads to a homogenization of the pressure distribution [22]. It also requires lower temperatures; especially there is no need for an additional sinter step, because a drying cycle is sufficient [22]. In contrast to that, the casting methods do not require a long-time heat treatment after a

controlled cool down phase to prevent residual stress or cracks [23, 42]. They offer a higher geometric freedom and level of detail than the pressing methods [37]. The low viscosity (e.g. 1 mPas for KCl-Na_2CO_3 [42]) of liquid salt grants a high shape accuracy and smooth surfaces. However, the geometry is restricted by the high shrinkage and the high coefficient of thermal expansion (CTE) of salt [24, 42]. The risks for void formation and thermal stress cracking increase together with wall thickness [20, 42]. Besides faster wash-out and material savings, this is probably another reason for the development of hollow-casted salt cores by gas injection technology [44, 60]. The tooling effort and the safety measures for liquid salt are more rigorous than for dry or wet salt powders, because of its higher reactivity and temperature.

Regarding the bending strength, the cast salt cores achieve the highest reported values. The reason is the beneficial particle reinforcement effect that occurs for hyper- or hypoeutectic mixtures of two or more salt species that was observed by many authors [20, 23, 24, 41, 42, 45, 53]. Cantas [53] found that a salt with a chloride (Cl^-) in the anionic part is more brittle than one with a carbonate (CO_3^{2-}), probably due to its larger dendritic structure.

1.2 Motivation

With the process loads of HPDC and injection molding being comparable, a lost core material that is viable in HPDC might be appropriate for the plastics industry, too. Suppliers from the automotive industry can ensure high production volumes, which makes the use of the existing salt core technology attractive for injection molding. The present article therefore investigates the application of commercial salt cores in injection molding and AFP with in-situ consolidation (isc). The motivation behind this is, to extend the capabilities of injection molding with the use of lost cores and local continuous fiber reinforcements. An incorporation of the two features will result in a higher geometric design freedom through the lost core and the ability to tailor stiffness, strength and damage tolerance for structural parts by continuous fiber reinforcements [61]. Successful overmolding experiments [62] with CF-PEEK injection molding compound and low-melting PAEK as matrix material encourage to investigate process routes that enable more complex aerospace parts. Both technologies can profit from each other through the process synthesis. The injection-molded part is locally reinforced with continuous fibers and the AFPisc laminate undergoes an additional temperature and consolidation cycle that can enhance its properties, for example, by compensation process-inherent flaws like poor crystallinity and consolidation of the last ply [63]. Therefore, the aim of this paper is twofold: At first, the viability of commercial salt cores will be investigated in injection molding. Second, the possibilities of a combination of salt core and continuous carbon fiber reinforcements applied by AFPisc will be elaborated, which will be the first base towards a “hybrid” insert for further overmolding.

The following research questions will clarify if commercial salt cores are appropriate for these tasks and how they can be modified to increase their usability for plastic processes:

- How can commercially available salt cores be incorporated in an injection molding process?
- What kind of preparation of commercially available salt cores is necessary so that they serve as substrate for continuous fiber reinforcements that are applied by AFPisc?

The performance of the current state of art salt core material will be shown in the following sections by processing and lab experiments.

2 SALT CORE APPLICATIONS IN PLASTIC AND COMPOSITE PROCESSES

2.1 Injection molding

2.1.1 Thin-walled, sintered salt cores in PA6 and CF-PEEK overmolding

2.1.1.1 Experimental part

The viability of the current salt core technology is investigated in injection molding experiments for PA6 and CF-PEEK. For the first tests, sintered salt cores are used that were provided by Emil Müller GmbH (Wilhermsdorf, Germany). The supplier does not disclose the process history or comprehensive material properties. It is assumed, that the provided salt specimens are similar to the material that was used in former investigations [22]. Table 2 sums up the available data.

Three-point bending strength [22]	22 °C	125 °C	250 °C
	12 MPa	9 MPa	4 MPa
Youngs modulus [22]	22 °C	125 °C	250 °C
	21 GPa	19 GPa	16 GPa
Density [22]	1.81 g/cm³		
Surface roughness R_z [22]	173 µm		
Heat capacity [22, 64]	853 J/(kgK)		
Heat conductivity [18]	6.39 W/(mK)		
CTE [18]	51.4E-6/K		
Melting point [18]	806 °C		
Material composition [18]	NaCl, purity > 96%		

Table 2: Material data attributed to salt cores of Emil Müller GmbH

The salt cores have a thickness of 2 mm so they can fit into the injection mold of a previous research project (Slokav, grant code: ZF4004305EB5) mounted on a KraussMaffei KM160CX injection molding machine. It is equipped with a screw with a diameter of 45 mm. The tool and the two-step injection process described below were originally designed for overmolding of thin continuous carbon fiber-reinforced PA6 and PEEK inserts. The salt core consists of three 66 mm x 20 mm x 2 mm segments that are bonded together with a cyanoacrylate adhesive (CA) via a butt joint. The salt core is placed without pre-heating in the cavity for the first shot, where it is overmolded with a supporting rib structure in a first injection. The rib structure stabilizes the core, ensures its proper alignment and fixation during the second injection that completely encapsulates the structure with polymer to form a rectangular bar with 222 mm in length, 25 mm in width and 5 mm in height. Figure 2 illustrates the process steps whereas Figure 3 shows the dedicated tool cavities and resulting parts.

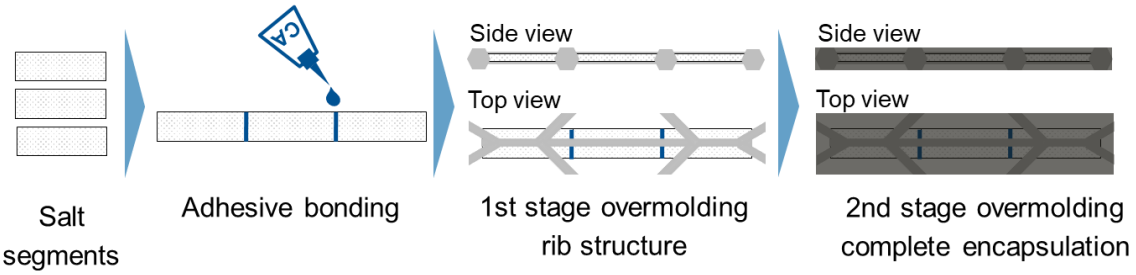

Figure 2: Project Slokav process route based on [65].

In order to save tooling effort, both cavities are placed in the same tool setup and can be activated by an inlet switch as required. The salt core has a wide support

in the tool and a short open span of 5 mm during the first injection, which represents the rib structure flow channel.

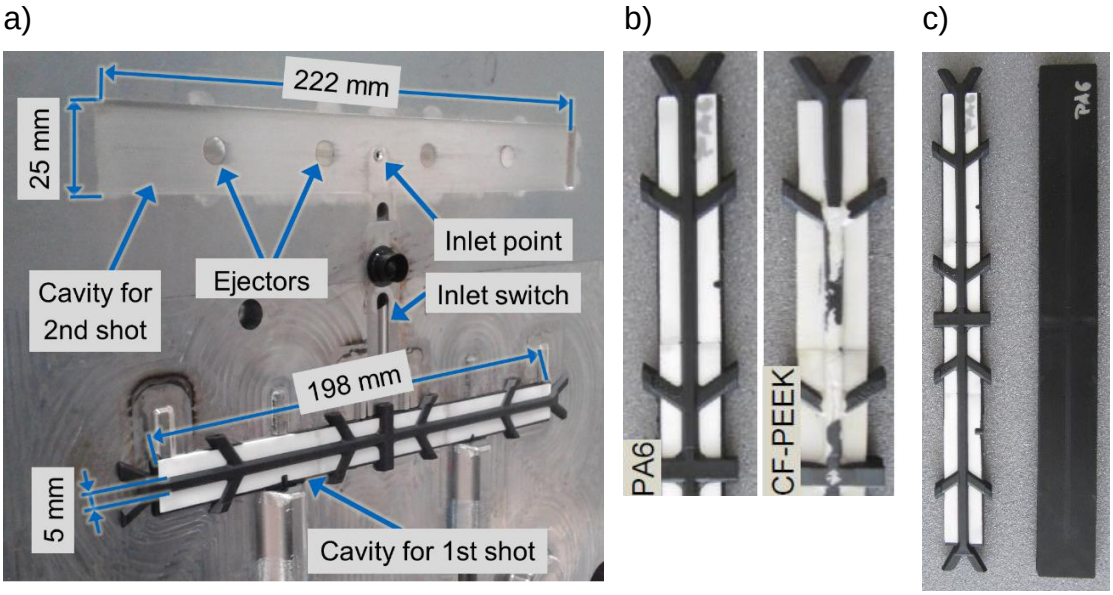

Figure 3: Slokav salt core trials: a) mold for 1st and 2nd shot; b) comparison of overmolded salt cores from 1st shot: PA6 (flawless) vs. CF-PEEK (failed); c) successful 1st and 2nd overmolding with PA6.

The injection parameters for the PA6 and the CF-PEEK are given in Table 3. Reduced injection speeds of 22 to 35 ccm/s were chosen for the second stage overmolding, because the salt core has less mold support in that phase. Five injection molding experiments are conducted for each of the two overmolding stages with PA6 and five for the first stage overmolding with CF-PEEK. A second stage overmolding with CF-PEEK was not possible, because of failure of the salt cores during the first stage.

Material	PA6	30% CF-PEEK
Product name	Schulamid 6 MV 14 black	Victrex PEEK 150CA30
$T_{salt\ core}$	23 °C	23 °C
T_{mold}	90 °C	210 °C
$T_{injection/nozzle}$	270 °C	380 °C
First stage overmolding		
Injection flow rate	100 ccm/s	50 - 60 ccm/s
Max. injection pressure	581 - 604 bar	1047 - 1456 bar
Second stage overmolding		
Injection flow rate	22 - 35 ccm/s	-
Max. injection pressure	323 - 439 bar	-

Table 3: Injection molding parameters for salt cores within project Slokav. The injection pressure is calculated from the hydraulic pressure of the injection unit.

Table 2 indicates a temperature sensitivity of the salt core strength for the temperatures during an injection cycle. Hence, a one-dimensional, transient thermal simulation estimates the temperature profile within the salt core as soon as it is placed in the tool, Figure 4. It is based on the standard transient heat transfer model for a plate with finite thickness and infinite dimensions in every other direction [66]. The model for the temperature distribution in thickness direction (x-direction) is described by equation (1),

$$\frac{\mathrm{T}(x,t)-\mathrm{T}_{\mathrm{mold}}}{\mathrm{T}_{\mathrm{salt\ core}}-\mathrm{T}_{\mathrm{mold}}}=\sum_{i=1}^{20}\frac{2\sin(m_i)}{m_i+\sin(m_i)\cos(m_i)}\cos\left(m_i\frac{x}{L}\right)e^{-m_i^2\,\tau} \tag{1}$$

with the eigenvalues m_i being calculated according to (2)

$$m_i=(2i-1)\frac{\pi}{2}\quad\text{for}\quad Bi\to\infty \tag{2}$$

and the dimensionless time τ being defined in (3),

$$\tau=\frac{\lambda\,t}{\rho\,c_p\,L^2} \tag{3}$$

wherein t is the time, λ the heat conductivity, ρ is the density, c_p is the heat capacity and L is the half thickness of the salt core. The first 20 eigenvalue terms of the exact solution are used in (1) which ensures a sufficient approximation quality for the original infinite sum [66]. The model inputs such as thermal properties and boundary conditions are taken from Table 2 and Table 3. The Biot number Bi is assumed to be infinite, because of the low heat conductivity of the

salt and its direct contact to the steel tool. The temperature at the interface between salt core surface and tool thus always matches the tool temperature. Due to the small dimensions of the salt core, the model assumption of infinite dimensions except thickness might not be justified. Furthermore, the small, contact-free zones due to the rib cavity are neglected. The model predicts a fast increase of the temperature in the center of the salt core. With a wall thickness of 2 mm, it reaches tool temperature in less than a second in both cases. The mold remains closed for at least five seconds before the injection. Therefore, the salt core is likely to be fully heated once the melt arrives. That is why it can be concluded, that the salt has a significantly lower strength, especially in case of the CF-PEEK injection, which is implied by its temperature sensitivity in Table 2. The dashed line in Figure 4b shows the temperature curve for an imaginary salt core with a thickness of 15 mm after five seconds. In this case, the temperature in the center remains below 125 °C. However, almost two-thirds of the thickness that are close to the tool are above 125 °C. This region will be prone to failure if bending moments are present, because mechanical stresses are the highest in the edge zone of the cross section.

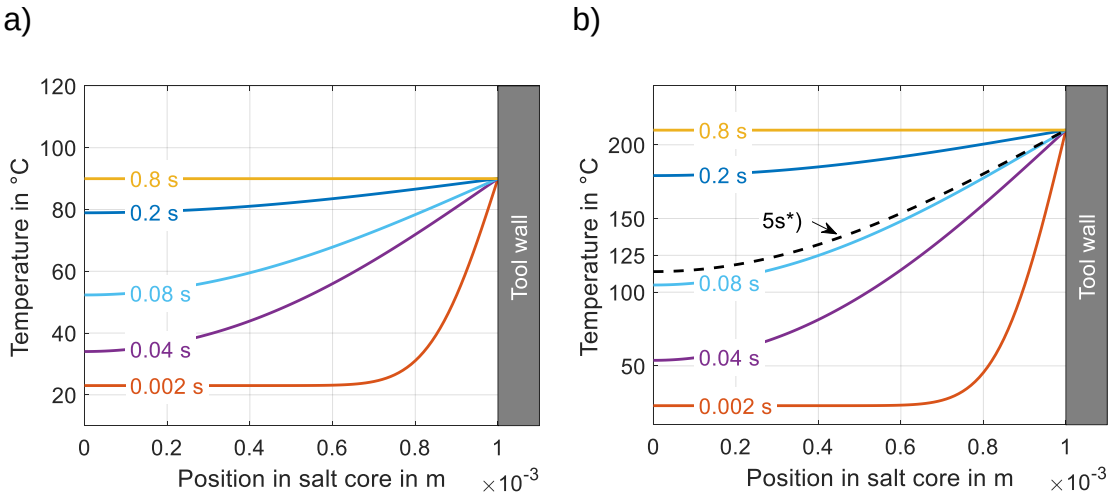

Figure 4: Simulated temperature distribution in thickness direction of a salt core that is placed in the Slokav mold for the first stage overmolding: a) T_{mold} = 90 °C of for PA6 injection and b) T_{mold} = 210 °C for CF-PEEK injection.
**) represents the temperature distribution in a half thickness of 7.5 mm, i.e. its temperature curve is scaled in the horizontal direction by factor 1/7.5 to fit it to the diagram.*
The center of the salt core is located on the left side of the diagrams and the tool contact is located on the right side.

The Slokav filling simulations with input data from Table 3 can be used to estimate the pressure loads on the salt core inserts (Figure 5). The PA6 simulations were

carried out with an injection flow rate of 100 ccm/s and the CF-PEEK simulations with a rate of 50 ccm/s. For complexity reduction, the inserts are modeled as rigid bodies like the tool. The simulations reveal that the flow front propagates almost parallel through the cavities on the inlet side and the counter side (Figure 5a). This leads to a mainly compressive load on the salt core, so it is not loaded in bending. The same effect can be observed for the second stage injection. Its final phase is shown in Figure 5b, which has a lower pressure profile in general. Therefore, the first stage injection must be considered the most critical for the salt core. Here, it must withstand pressures up to 43 MPa close to the inlet [65]. The results of the CF-PEEK simulation show a similar behavior. Again, the first stage injection is more critical. The highest cavity pressure in the second stage injection is predicted to be approximately 42 MPa close to the inlet [67]. According to Figure 5c, the first phase of the CF-PEEK injection causes the highest pressures up to 73 MPa in the cavity, but the melt fronts are also aligned almost in parallel [67], which is assumed to be advantageous for the salt core viability.

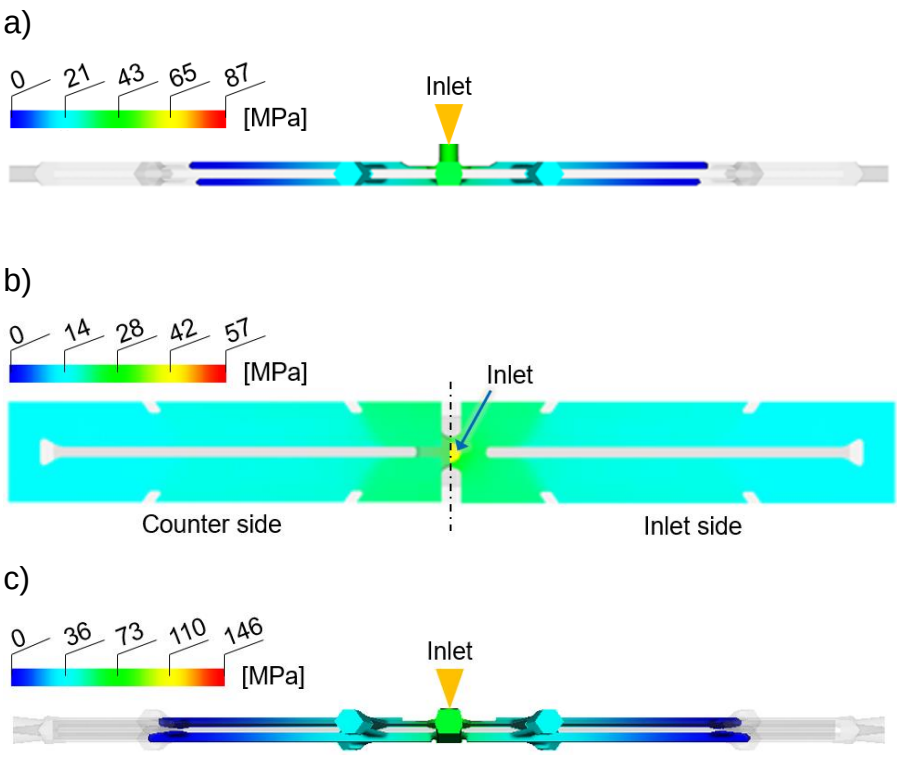

Figure 5: Pressure profiles of Slokav filling simulations: a) first stage PA6 (based on [65]), b) second stage PA6 (based on [65]) and c) first stage CF-PEEK (based on [67]). The results were obtained with Autodesk Moldflow Insight 2017.

The injection molding experiments with PA6 achieve a complete filling without defects (Figure 3c). A specimen with a length of 20 mm is cut from the center of the rectangular bar. The salt dissolves completely in a still water bath of 300 ml

without showing contamination that might hinder the salt powder restoration by evaporation and subsequent grinding. The resulting cavity shows a good accuracy and is residue-free (Figure 6). The dent in the top section of Figure 6 is likely to be an air entrapment when the melt encapsulated the rib structure, rather than a salt core defect.

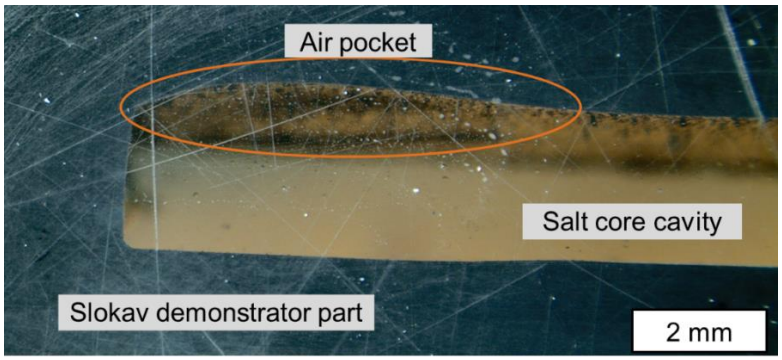

Figure 6: Slokav PA6 specimen after wash-out of the salt core: Due to the air entrapment, the geometry deviates from the desired rectangular cross section on the left upper edge [68].

2.1.1.2 Discussion

From the experiments, it can be concluded, that the salt core withstands process loads imposed by an injection flow rate of 100 ccm/s and the corresponding pressures for PA6. It has to be noted, that Table 3 provides the injection pressure close to the nozzle section of the injection molding machine. The melt hits the salt core with a lower pressure of 43 MPa that is predicted by the filling simulation. At this point, the salt core is heated to the mold temperature of 90 °C according to the thermal simulation. Although the salt core does not have its full strength due to its temperature sensitivity, the injection strategy of parallel flow fronts on its top and bottom side is successful. The salt core survives the critical first stage overmolding and is then stabilized by the rib structure for the second stage overmolding.

In contrast to that, the first stage CF-PEEK injections destroy the salt core. The first stage of CF-PEEK overmolding requires an injection flow rate of 50 ccm/s to avoid short shots. The filled PEEK grade has a worse flow behavior than the PA6, which becomes evident in higher pressures that are needed to fill the cavity (Table 3, Figure 5c). According to Table 2 and Figure 4b, a severe drop of strength must be expected at elevated temperatures that are caused by heat transfer from mold and melt. Weakened by the high temperature, the salt core is pushed in the counter mold part that is facing away from the inlet (Figure 3b, Figure 7). Thus, flashes can be observed alongside the ribs on the inlet side because of increased gaps between tool and salt core. Deformed salt and salt fragments block the main flow channel on the counter side that was supposed to

be filled via the central runner rib. The melt must then take the longer path through the outer ribs in order to arrive at the counter side. This results in a scrap part that cannot be further processed.

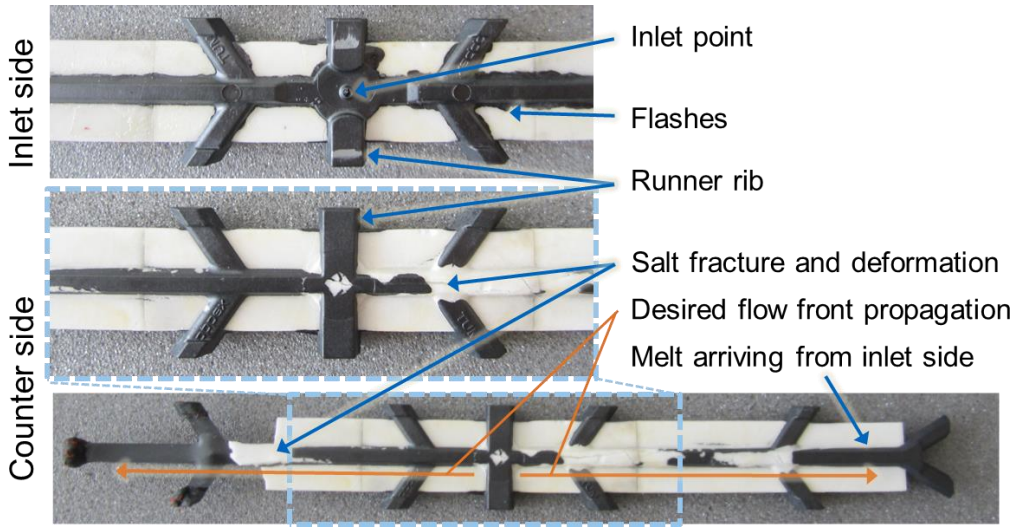

Figure 7: Detailed view on salt core that is broken and deformed by the CF-PEEK melt.

The filling simulations do not take into account the thermo-mechanical behavior of the salt core. Furthermore, detailed, temperature-dependent data are not available to the authors. The simulation fails to predict the loads during the CF-PEEK injection, because the actual cavity geometry changes due to the salt core deformation. Therefore, it is not possible to formulate design criteria based on the current experiments. For example, if a salt core with a higher thickness of 15 mm is considered in the thermal model (Figure 4b), the center of the core stays at temperatures below 125 °C for a longer time, at which point the salt core will achieve 75% of its bending strength (Table 2). However, two-thirds of the thickness are heated above that temperature and it is questionable if even such a bulky salt core could withstand the process loads, especially if they impose stresses that are critical for the weakened edge zone, for example bending or shear stresses.

To sum up, the salt core experiments within project Slokav demonstrate the capabilities and limits of commercial, sintered salt cores with a thickness of 2 mm. They are used to gain experience of the injection molding behavior of the salt material. They are a proof of concept for the designed filling behavior in the two-stage overmolding process for PA6. However, they are not suitable in their present form for CF-PEEK injections. A much higher wall thickness is required in order to avoid a widespread loss of mechanical performance that is caused by a temporary exposure to 210 °C in the mold.

2.1.2 Thick-walled, casted salt cores in CF-PEEK overmolding

2.1.2.1 Experimental part

In the Clean Sky 2 project IMCoLoR (Injection Molding with Continuous Local Reinforcements, grant agreement ID: 738131) [69], the aim was to build a circular demonstrator part with a U-shaped cross section in a two-step overmolding process. Its dimensions are approximately 270 mm on the outer diameter, 135 mm on the inner diameter and 150 mm in length. A model of the part components is shown in Figure 8a. The demonstrator part consists of a CFRP insert, which is made of the low-melting CF-PAEK tape Toray (formerly TenCate) Cetex TC1225 (Table 4), and two subparts from the first and second injection that are joined via overmolding with CF-PEEK.

A casted salt core, made on a 400 t HPDC machine by Aluwag AG, Suisse, enables the undercut (Figure 8a). The supplier does not disclose the process history or material data for the salt. It is assumed, that the casted salt segments are based on a KCl-Na_2CO_3 mixture which is proposed by Bühler AG [42]. Table 5 sums up the available data. It has to be noted, that the bending strength of casted composite salts strongly decreases with elevated temperatures similar to that of pressed and sintered salt. This is shown in experiments of Fickel [24] and Oikawa [48]. Although these authors used other salt mixtures, it is assumed that the salt material for IMCoLoR has a similar temperature dependency. There are no bending tests for the salt material, which was provided by Aluwag AG.

Fiber areal weight	145 g/m²
Resin content per weight	34%
Density	1.59 g/cm³
T_{melt}	305 °C

Table 4: Properties of Toray Cetex TC1225 UD tape material [70]

Three-point bending strength [42]	23 - 39 MPa	
Density [42]	2.33 g/cm³	
Heat conductivity [42]	2.2 W/(mK)	
CTE [42]	20 °C	500 °C
	20E-6/K	60E-6/K
Melting point [71]	581 °C	
Material composition [42]	KCl (38%) + Na_2CO_3 (62%)	

Table 5: Material data attributed to salt cores for IMCoLoR

Because of the high salt shrinkage, it is not possible to produce segments bigger than 180°. Otherwise, the segment would build up cracks. Furthermore, the undercut geometry of the PEEK part requires a vast salt accumulation that is prone to casting defects. In order to mitigate the risks, the maximum core thickness is set to 35 mm, the minimum thickness is set to 20 mm, the segmentation angle is set to 90° and several material cutouts from a rib-like structure on the inside, Figure 8b. The salt core segments are bonded to each other and mounted together with the subpart from the first injection on the salt core carrier. This results in a compact insert for the second injection and facilitates handling. The segments are bonded by the high temperature epoxy DELO Duopox SJ8665. The bond lines are clearly visible as dark lines in the CT scans Figure 9. Apart from sanding with 120 grit paper and subsequent vacuum cleaning, there is no surface treatment.

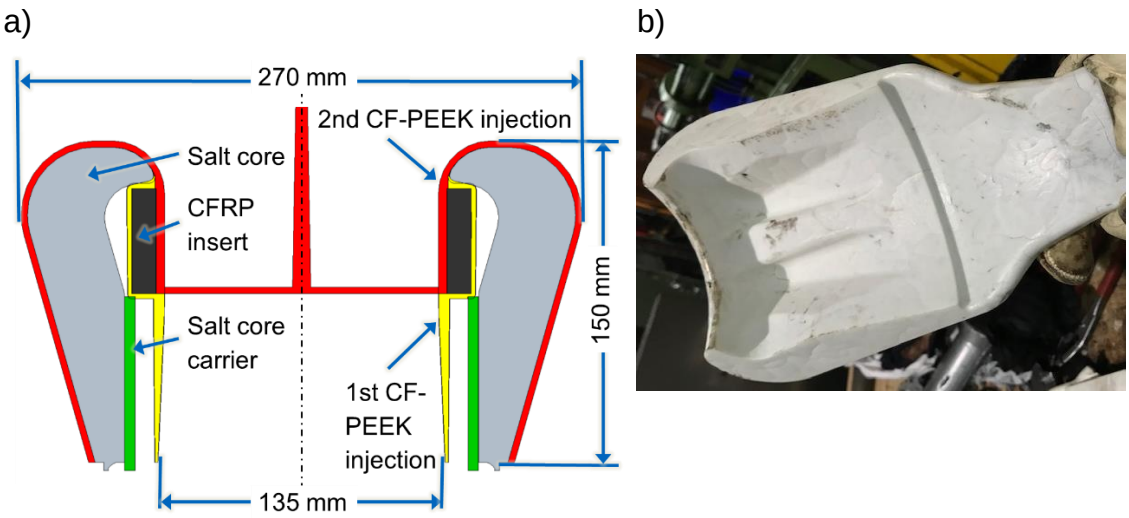

Figure 8: a) Schematic cross section of the IMCoLoR demonstrator part and b) 90° salt core segment.

The salt core segments suffer from casting defects, as the CT scans reveal, Figure 9. Most of the segments have a high void content (z = 80 mm, Figure 9a). The voids grow bigger in circumferential direction with decreasing z position (z = 35mm, Figure 9b) which leads to an actual wall thickness of 7 mm instead of the designed thickness of 33 mm in that section. This is especially critical, because there the PEEK melt front will meet the salt surface for the first time during the injection. Furthermore, shrinkage cracks can be observed in most of the segments and they do not match the inner radius for a proper fit on the overmolded CFRP insert (first shot CF-PEEK in Figure 8a). Hence, the segment geometry exceeds into the cavity where it causes flow path constrictions. The center rib has no contact to the insert, which results in a lack of support against pressure or bending loads. Another problem resulting from the misfit are gaps between the segments of up to 10 mm. These problems emerge from the high

material accumulation in the rib sections and a premature freeze-off during the salt casting. The filling behavior could have been improved in subsequent salt casting cycles. However, the project resources were not sufficient to afford additional salt casting iterations.

a)

b)

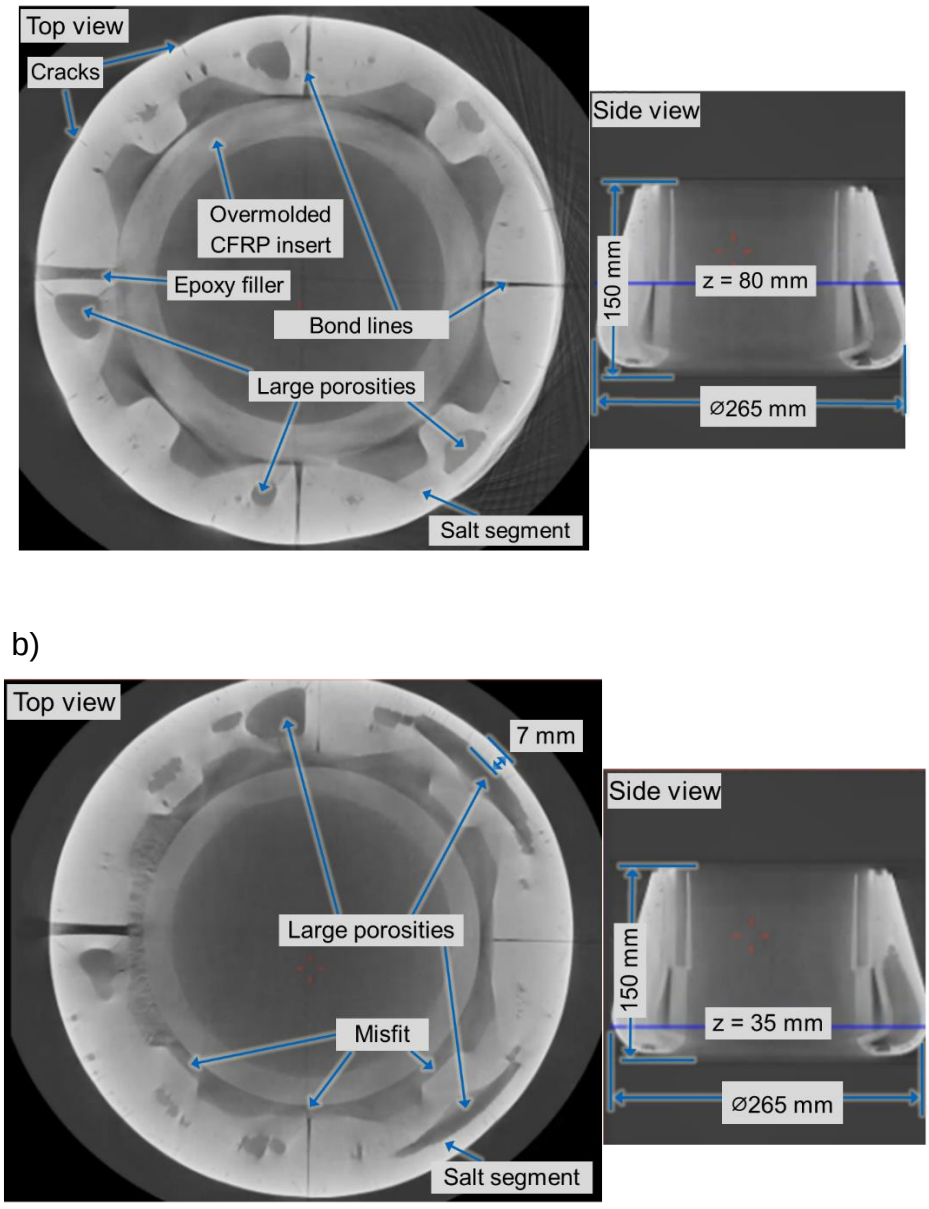

Figure 9: CT scan of a salt core made by HPDC: a) z-position = 80 mm, b) z-position = 35 mm.

In order to use these salt cores for the secondary injection of the two-step injection process, the biggest voids are filled with a low viscous resin, namely

Sika Biresin CR80/CH10, to backfill the most critical structure close to the inlet system.

The injections are conducted on a KraussMaffei GX650 injection molding machine at KraussMaffei Technologies GmbH, Munich. It is equipped with a screw with a diameter of 80 mm. In total, there are 14 injection trials. Table 6 lists the machine settings and Figure 11 shows the packing profiles of the most successful injections, i.e. wherein the melt reached the outmost region of the mold (KM11 to KM14). Prior to the CF-PEEK injection, the assembly of salt core and insert is heated in an oven to a rather low temperature of 60 °C, in an effort to prevent stresses due to thermal expansion mismatches of the material mix (e.g. salt, aluminum, CF-PEEK, epoxy) and a temperature-induced loss of strength of the material.

Material	30% CF-PEEK
Product name	Victrex PEEK 150CA30
T_{mold}	215 °C
$T_{injection/nozzle}$	395 °C
$T_{salt\ core}$	60 °C

Table 6: Injection parameters for salt core overmolding in IMCoLoR

The initial injections KM01 to KM10 show that the flow channel constriction always leads to an incomplete filling behavior although the injection flow rate was set to the minimum of 200 ccm/s, Figure 10a. In order to ease the flow front progress, grooves are cut in the segments, which provide an alternative flow path for the melt, Figure 10b. All salt cores starting from KM11 are modified in this way. This pragmatic geometric adaption in combination with an injection flow rate setpoint of 600 ccm/s enables the melt to reach the end of the cavity.

a) b)

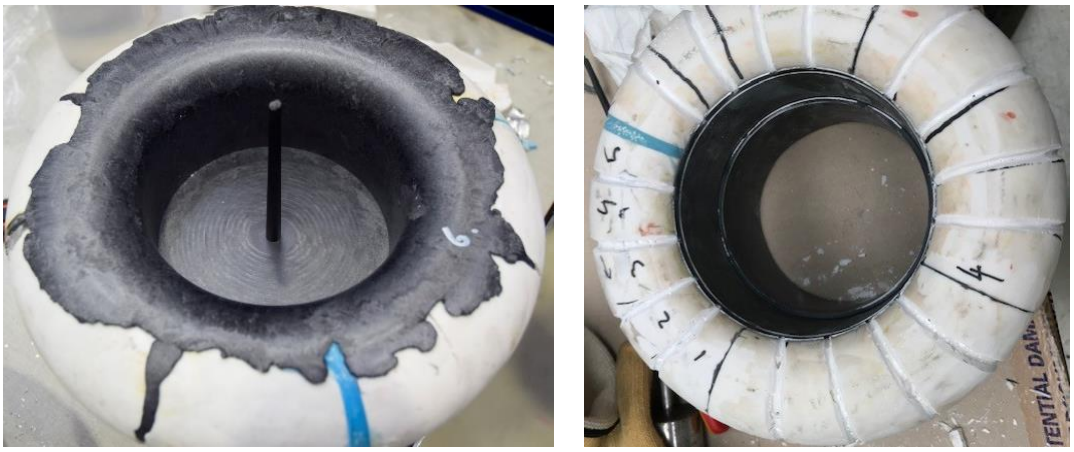

Figure 10: a) Stuck flow front on an original salt core; b) Countermeasure: grooves provide alternative flow paths.

However, there are flashes of several centimeters located in the undercut region of the part. Furthermore, there are flashes in radial direction that partially connect the outside and the inside of the cavity. Salt fragments block the cavity and prevent the progress of melt flow, which further increases the pressure on and within the core. These effects result from the salt core. There are parts of the designed cavity, which are filled with CF-PEEK because the epoxy filler did not reach every hollow section. The adhesive bonded joints between the salt core segments were not dense and tough enough to prevent the melt from entering the adhesive gap and causing flashes there, too. The structural flaws caused the salt cores to crack, break and fill with polymer.

The injection flow rate and pressure curves (Figure 11) clearly deviate from the ideal which should have a plateau after the first peak for the packing phase [3]. The present curves do not match with that ideal, because of the broken salt core segments. It is assumed, that KM11 and KM12 fail early in the filling phase i.e. at lower pressures, because the pressure slowly increases and the injection flow rate decreases slowly as the core cavities are filled. For KM13 and KM14 it seems like the cracking happened later in the filling phase. The sudden failure of the salt core under high pressure opens up a new cavity for the melt, which causes instabilities of the machine control. The curves of the flow rate and pressure show large oscillations. Therefore, a proper packing phase is not achieved.

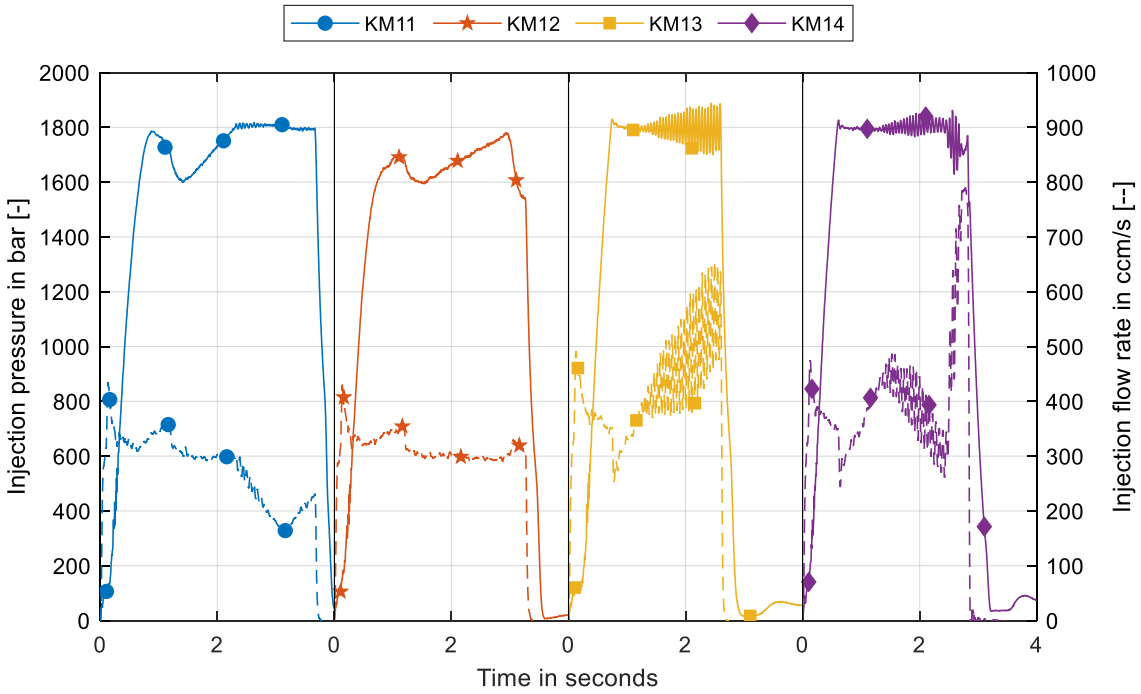

Figure 11: Packing profiles for the most successful injections (KM11 to KM14) within the IMCoLoR series.
The injection pressure is calculated from the hydraulic pressure of the injection unit and is indicated by the solid line [-]. The injection flow rate is indicated by the dashed line [--].

Part KM13 shows the best results throughout the test series. After the salt was removed by immersion in a bath in a 50 l water tank for 24 h and cleaning by a pressure washer, the CT scan reveals that there are cross sections, which kept the contour of the desired geometry quite well (highlighted section in Figure 12). In this section of the demonstrator part, an almost flawless salt core segment was installed that withstood the injection loads. In contrast to the other 75% of the circumference, there are no gaps on the outside of the part or massive flashes on the inside. For all other parts, the abovementioned defects occur for 100% of the circumference.

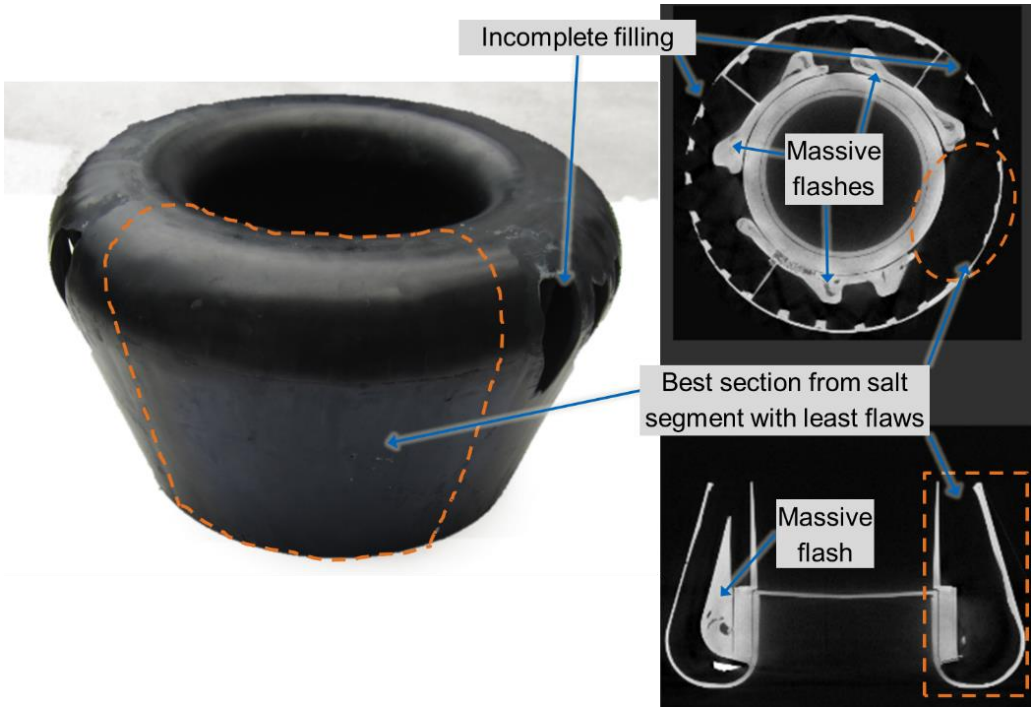

Figure 12: IMCoLoR demonstrator part KM13 with top and side view of its CT scan. The salt has been completely removed. The section highlighted by the dashed line shows the best geometric accuracy of all salt segments that were employed throughout the test series.

2.1.2.2 Discussion

The KM13 experiment shows that casted salt cores have a potential to be used in CF-PEEK injections. Although the unbroken segment proves that salt can withstand the process loads with the chosen geometry, there are still some challenges to overcome. The production of salt core segments of sufficient quality must be ensured. Additional iterations should be conducted to refine the salt casting tool and process. Especially, the filling method has to be reworked, because it is prone to produce faulty segments due to a prematurely frozen layer close to the inlet which results in large porosities (Figure 9 and Figure 13a). In order to avoid this, the authors suggest an alternative filling method in Figure 13b. The salt melt should enter the cavity at the thickest part and then exit thorough two outlets. The outlets should be located at the thinnest cross sections that are far away from each other. This should maintain a steady melt flow until the segment cavity is completely filled. The geometric misfit can be compensated by tool iterations once sound segments are produced.

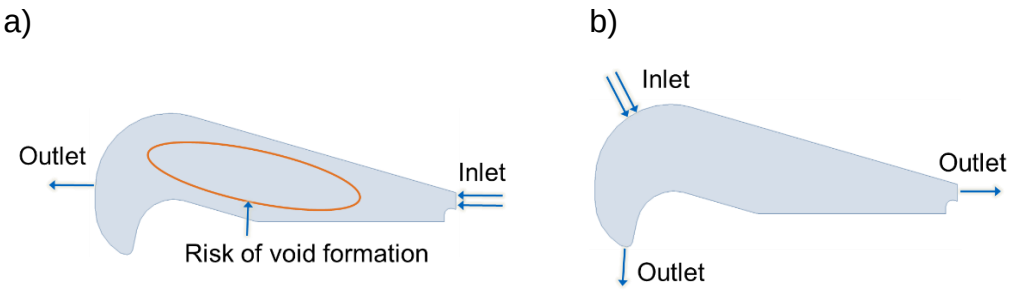

Figure 13: a) IMCoLoR original salt core design and b) design improvement suggested by the authors.

Furthermore, the time-consuming assembly could be saved with another joint strategy for the segment assembly. For example, a jig-saw connection as it is suggested by Kaerger [40] for a binder-stabilized sand material could be an possibility for salt cores, too. The absence of bond lines would ease the cleaning of the parts, because there are no more water-insoluble components in the cavity.

2.2 AFPisc of CF-PEEK tapes

2.2.1 The AFPisc process

The principle of an AFPisc process is shown in Figure 14. A thermoplastic tape is guided through a feeding and cutting unit (not shown) towards the consolidation roller that presses the tape on the substrate. The whole placement unit moves relatively to the substrate surface while an infrared (IR) laser heats the incoming tape and substrate in front of the consolidation roller. The materials merge in the nip point. The closed-loop control is guided by the feedback of the thermal imaging camera. It aims for a homogenous tape and substrate temperature and tries to meet the user-specified nip point temperature. The control unit thus regulates the temperature distribution with the angle of incidence and the laser power in order to enable a good bond.

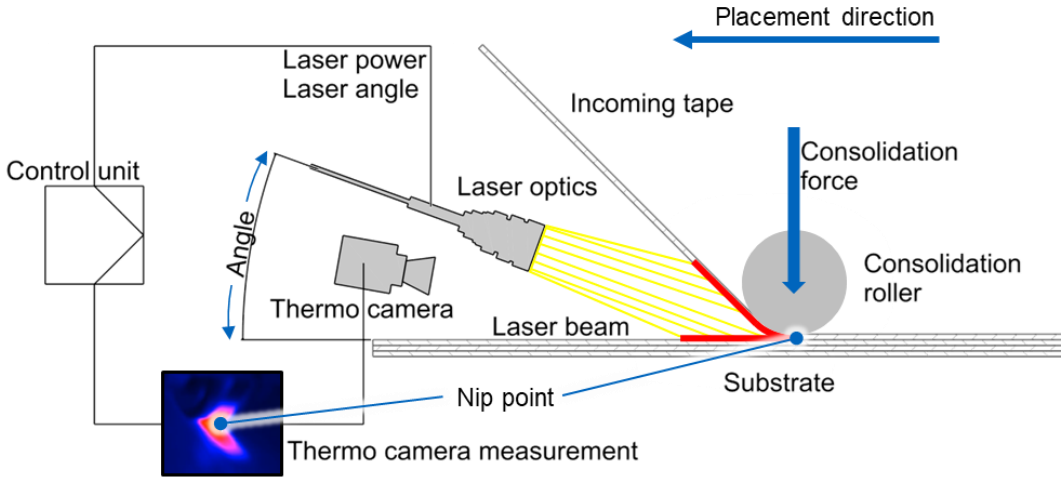

Figure 14: Principle of the AFPisc process (adapted from [72]).

2.2.2 Increasing first layer adhesion with spray or foil coating

A successful bond between a robust salt core and the first layer of a composite structure manufactured by AFPisc would extend the design freedom beyond the state of art [73] where a water-soluble, expendable filler material is used to solely provide an even, compression-resistant surface for tape placement. A “hybrid” insert for injection molding, which is made of thermoplastic CFRP and salt components based on a material presented in Table 1, will open new possibilities in subsequent processing. A good adhesion between AFPisc laminate and salt core will increase its handling stability and - depending on the geometry - may reinforce fragile salt segments during overmolding. Furthermore, a CFRP insert would be less prone to deformation or displacement during an injection once it is tied to the salt core.

However, the first layer adhesion is weak for tapes with a low matrix content such as the Toray Cetex TC1225 (Table 4). First tests show a bad adhesion between the salt and tape when salt surface is left original or only sanded with 120 grain [68]. Therefore, the aim of the next experiments is to check suitable surface preparation methods. The same salt bars as for the Slokav trials (Table 2) are used throughout the test series due to their lower price and higher availability than casted salt bars.

Two approaches are investigated: spray coating and foil coating of a thin salt specimen with dimensions of 66 mm x 20 mm x 2 mm. The foil coating consists of three layers of a 100 µm PEEK foil of Victrex APTIV 1000 Series Films. Its melting point is specified to be 343 °C [74]. A vacuum-assisted press applies 12 bar consolidation pressure at 360 °C. Vacuum is engaged to avoid porosity in between the layers and the adhesion zone. The dwell time at target temperature is 5 to 10 min, followed by a cool down of 2 h while maintaining the pressure.

The spray coating incorporates the PEEK dispersion Victrex Vicote F804 [75]. It is manually applied via an airbrush with a 0.8 mm nozzle and pressure of 3 bar. The setup is dried at room temperature for 5 min, in an oven at 120 °C for 18 h and kept above melt temperature at 380 °C and 400 °C for a dwell time of 10 min. The specimen cool down to room temperature in the oven afterwards.

The foil coating has a smooth and porosity-free surface. The mean layer thickness is 275 µm, Figure 15a. Excessive material is squeezed to the side because of the simple plate tool. The foil coating shows a good adhesion, but the reduced stiffness and plastification of salt at higher temperatures in combination with the different shrinkage characteristics of PEEK result in a residual stress deformation, Figure 15b. In contrast to that, the spray coating achieves a thinner layer with a thickness of 70 µm to 80 µm, Figure 16a. The thickness is harder to control due to the manual spray coating. The spray-coated specimens do not show any deformation after drying.

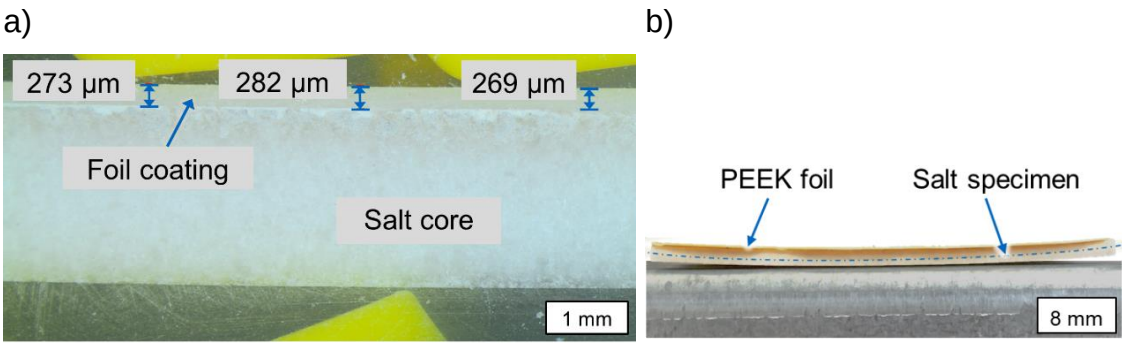

Figure 15: a) Foil coating layer thickness and b) specimen warpage [76].

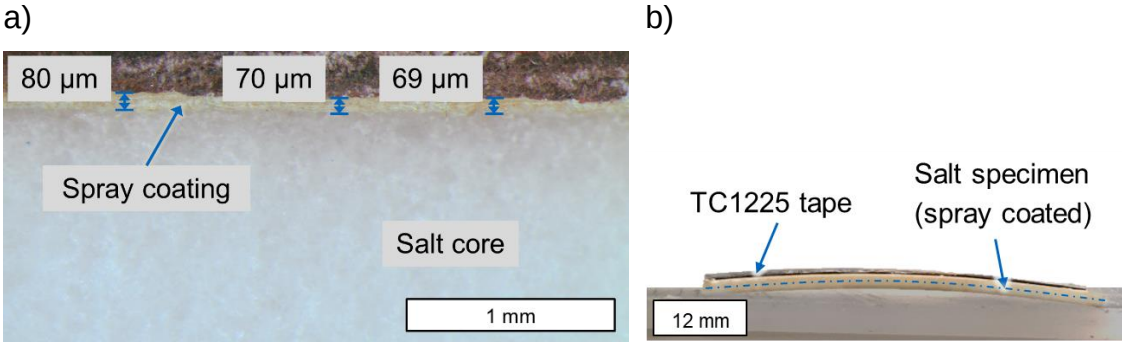

Figure 16: a) Spray coating layer thickness and b) specimen warpage after hot pressing of TC1225 [76].

One layer of TC1225 with an initial width of 12.7 mm is attached to the prepared salt specimens. In a first experiment, the tape is fused to the specimen by the same press process as for the foil coating. With the TC1225 tape attached, the specimen deform in the opposite direction as for the foil coating, Figure 16b. In

order to ease handling and to stabilize the thin salt specimen for further tests, they are bonded to a metal plate carrier with DELO-DUOPOX SJ8665 epoxy adhesive.

In a further experiment, AFPisc is used to place the TC1225 tape on the surface. Several metal sheets ensure an even placement path for the consolidation roller before and after the salt specimen (Figure 17). The AFPT machine was set to a nip point temperature of 460 °C for the closed-loop laser control, a drum pressure of 1.5 bar (equals 187 N or 19 kg consolidation force) for the consolidation roller at a placement speed of 3 m/min.

The tape width after placement is 14 mm for both substrates. The tape width enlargement is a result of the squeeze-flow in the compression phase and an indicator for the consolidation quality. However, the current AFPisc technology does not meet the consolidation quality of press or autoclave processes yet [63]. Up to 48% of increase in tape width are observed for consolidation forces of 40 kg for CF-PEEK tapes and attempts are made to maximize the tape width enlargement for a better mechanical performance [77]. Therefore, the increased tape width of 16 mm after hot-press bonding on the foil-coated surface is in line with the expectations drawn from the state of art. In contrast to that, the hot-press bonding on the dispersion-coated surface results in 14 mm tape width on the substrate. The reason is likely a hindered matrix percolation, which is a main driver for the squeeze-flow [63], due to lower matrix content that is provided by the dispersion coating compared to the foil coating.

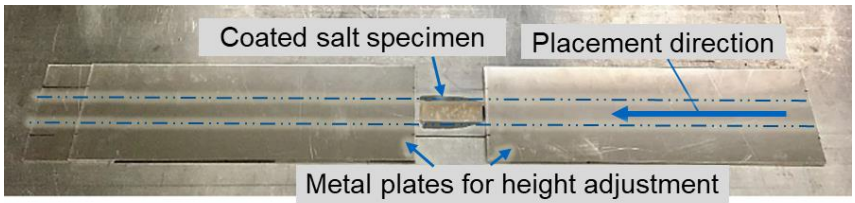

Figure 17: Setup for AFPisc placement of 12.7 mm tapes on a PEEK coated salt specimen.

2.2.3 Peel test setup

A Hegewald & Peschke inspect100 universal test machine is used to carry out the peel tests. The force is measured by a 1-kN load cell. The crosshead speed is set to 50 mm/min. The expected forces are low and the expected displacements are high, hence the position signal of the machine sufficiently represents the travel without the need for an optical determination. Figure 18 shows the test setup at the beginning. The specimen carrier is clamped on a movable platform while the free end of the tape is connected to the force cell. The test rig has a variable peel angle which was originally designed for peel ply tests [78]. The peel angle is set to the minimum of 90° to avoid premature failure of the

carbon fiber tapes due to too small bending radii. The moveable platform is linked to the crosshead via steel cables that maintain the peel angle through a compensation of the vertical by a horizontal displacement.

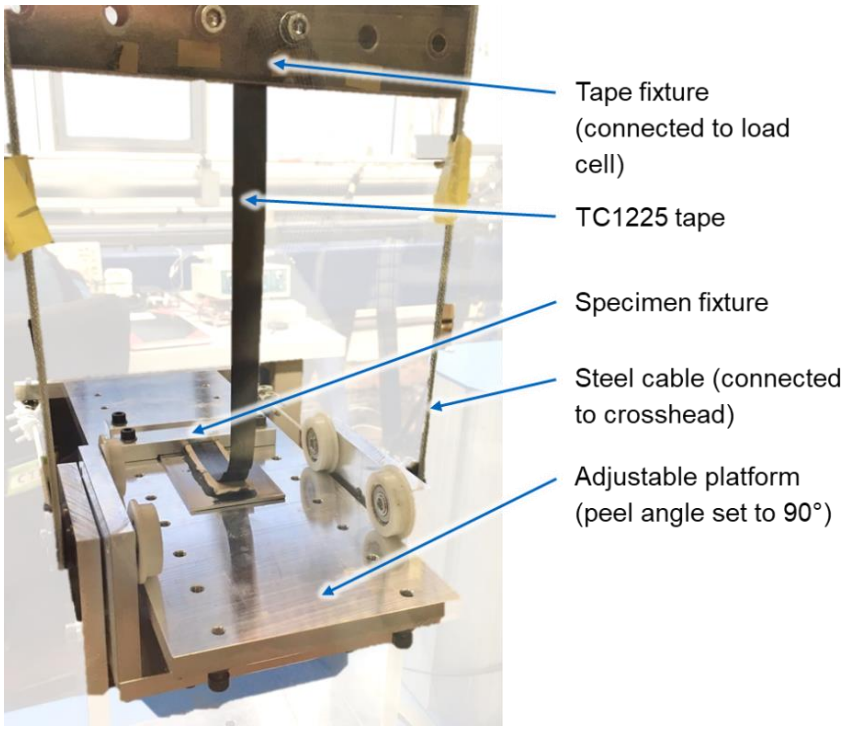

Figure 18: Peel test setup

2.2.4 Peel test results

The foil coated and then hot pressed specimen (FC-HP) have the highest peel resistance with maxima higher than 17 N. Figure 19 reveals that specimens FC-HP_2 to FC-HP_4 broke at the very beginning without any peel failure because the tape broke first. In these cases the TC1225 tapes could not bear higher loads for the 90° bending angle. Besides, the tapes exhibit imprints from the edge of the press tool and show an over compaction close to the front of the specimen. These effects might contribute to a lower resitstance of the tapes while they are peeled off. In contrast to that, the failure mode for specimen FC-HP_1 and FC-HP_5 is cohesive in the salt and ahdesive on the salt-foil coating interface, repsectively. I.e. the adhesion strength between tape and foil coating is higher than between foil coating and salt. The majority of FC-HP bonds fail due to cohesion of the tape or the salt itself and not due to adhesive defects. Therefore, the FC-HP results can be seen as a benchmark for the whole test series.

The failure mode of the dispersion spray coated and then hot pressed (DC-HP) specimen is a combination of adhesvie failures between the coating and the salt and an ahesive failure between the tape and the spray coating over the whole

specimen length, Figure 19. The highest peel forces occure right at the beginning where the salt spray coating interface fails first. After that, the failure mode splits up and the peel force decreases. It is assumed, that the high forces in the beginning are an effect of the overcompaction of the tape, which could be observed for the foil coating, too. However the adhesion of the spray coating to the salt is not strong enough to withstand the peel forces until the tapes break.

All foil coated and AFPisc processed specimen (FC-AFP) except FC-AFP_3 show adhesive failure between tape and coating, followed by a failure of the tape, Figure 19. For FC-AFP_3, the foil coating peels off the salt at very low forces including salt fragments, which represents a mainly cohesive failure of the salt itself. From the AFPisc point of view, this might be the preferred failure mode, because the substrate fails first. However, the maximum force is much lower (< 4 N) than for the other specimens (> 10 N) which is why FC-AFP_3 is assumed to be an outlier with a probably pre-damaged salt specimen. In general, a bad adhesion can be observed between tape and foil coating on the first 10 mm to 20 mm of the placement path on the specimen. The reason for this is likely to be the laser control. There is a sudden change of material properties from metal to PEEK foil, which has different thermal and optical properties. The laser control cannot adjust the heating profile fast enough, so the first millimeters are lost in terms of optimal heating and bonding. Evidence is found in the thermal camera signals, which are fed back to the laser control, Figure 20. While the temperature of ply (=substrate), tape and nip point (=control temperature) are in a range for sufficient bonding on the specimen track, the temperatures in the transition region from metal to salt surface are lower. The adaption of laser power and the inclination angle of the laser, which shall ensure an adequate temperature distribution for tape and substrate, needs some time to settle.

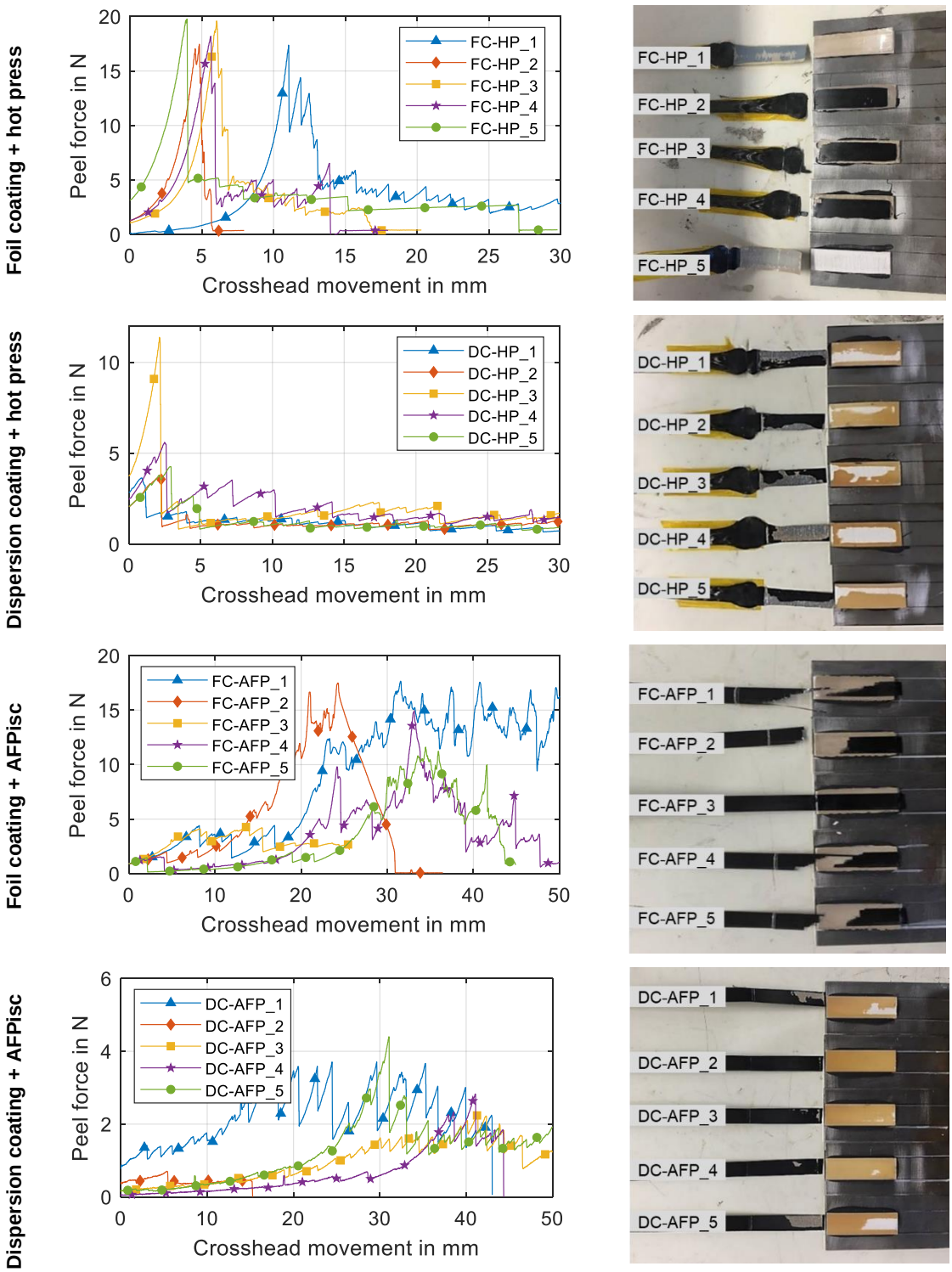

Figure 19: Peel curves and peel specimen of the sets FC-HP, DC-HP, FC-AFP and DC-AFP [76].

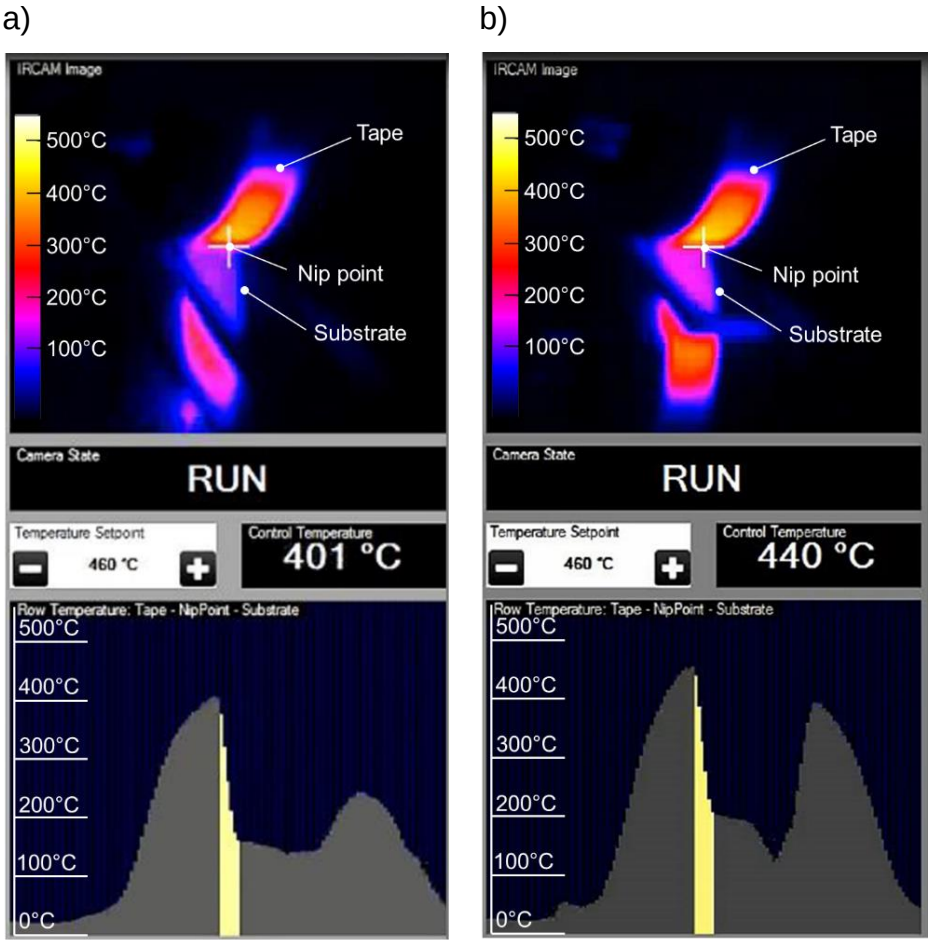

Figure 20: Thermal imaging of laser absorption or heat distribution, respectively, during the layup a) near the gap between metal sheet and salt core and b) close to the end of the salt core. The bottom graphs show the heat profile under the consolidation roller: left side = incoming tape, yellow center = nip point, right side = substrate.

Low peel forces (< 4.5 N, Figure 19) are observed for the specimen sprayed with the dispersion and then processed in AFPisc (DC-AFP). Adhesive failure occurs between spray coating and tape, again at the beginning of the specimen track. Specimen DC-AFP_4 fails completely adhesive between tape and coating. The other specimen show partial adhesive failure between the coating and the salt surface and bear slightly higher peel loads. These experiments are in line with the foil coating results, where the strength of the tape-to-coating interface is higher towards the end than close to the beginning of the placement path.

2.2.5 Discussion

The adhesion between foil coating and tape is better in general. Those specimens achieve the highest peel resistance, likely because of the higher matrix content that is provided by the foil coating. In contrast to that, spray coated specimen have the lowest adhesion strength for both consolidation methods, AFPisc and press. The failure characteristics are similar and the peel force as well as the increase in tape width are low. This indicates a poor consolidation and poor adhesive bond. The pressed specimen have a higher peel strength than AFPisc specimen. The reason is probably the longer dwell time and a more homogenous pressure and temperature distribution, which allows the material to form a better bond. This could also be expected from the abovementioned increased tape width for the foil-coated specimen. However, the tape width effect is weaker for the spray coating. It is assumed that the low matrix content hinders the squeeze-flow and bonding mechanisms.

It has to be noted, that the tape width for AFPisc is the same for both types of the coating whereas there is a distinct difference for the press method. The AFPisc cannot make use of the increased squeeze-flow potential that is offered by the foil coating. Apart from the lower consolidation force compared to the press, probably the abovementioned problem with heat distribution from the laser control is a reason for that.

The higher scatter of AFPisc specimen and intensified adhesion failures at the beginning of the placement path on salt core indicates an unstable processing especially in the transition zone from metal to salt (Figure 19). The adjustment of the laser control is not fast enough to address the sudden change of the substrate at a placement speed of 3 m/min. Figure 20a reveals, that the melting temperature of PEEK is not reached for the substrate close to the nip point. Even close to the end of the salt core, the substrate temperature is still around 200 °C (Figure 20b). The bond therefore forms only due to the molten matrix fraction of the incoming tape, which results in weaker bonds. Coordinate based control methods [72, 73] should be preferred to ensure a uniform temperature distribution in such cases. I.e. the closed-loop control unit is temporarily disabled while a knowledge-based lookup table sets the machine parameters (Figure 21). Another aspect is the optical behavior of the substrate. Neat PEEK [79] as well as NaCl [80] transmit laser light in the infrared spectrum. The energy absorption is thus mainly caused by the carbon fiber during AFPisc [79]. The heat input could be improved by adding absorptive particles to the irradiated surface of salt core (Figure 21) or by its pre-heating via the tool or in an oven.

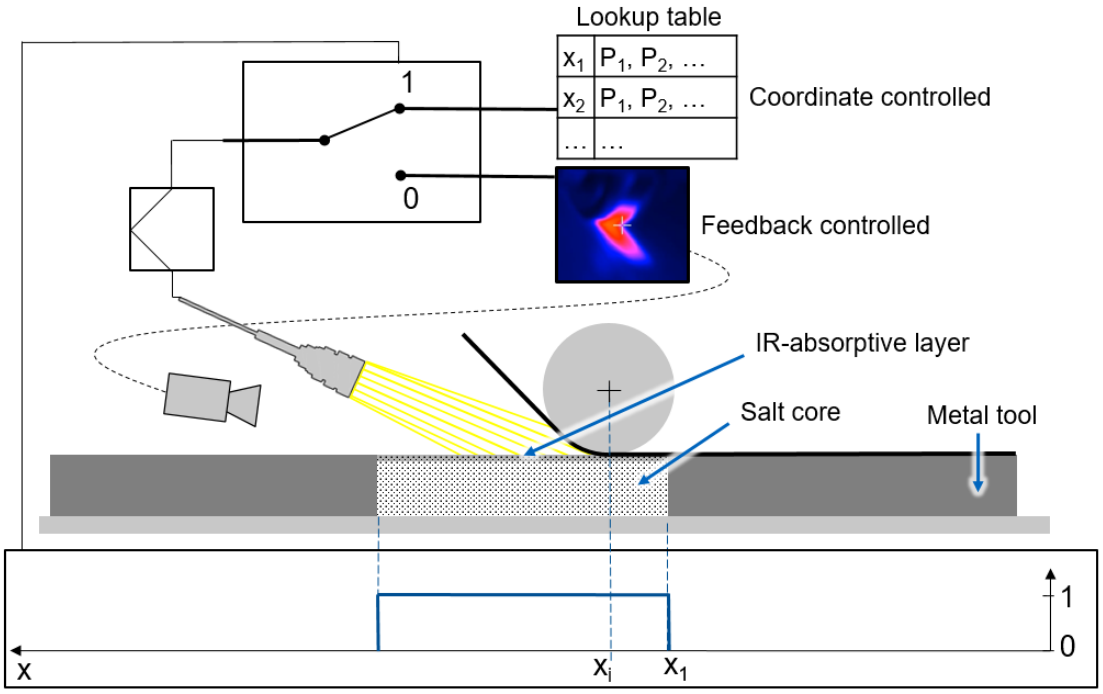

Figure 21: Suggested modifications for improved first layer adhesion between salt core and tape during the AFPisc process.

However, both coating methods already lead to an improved first layer adhesion compared to a virgin salt core surface. The peel forces are just 0.5 N without surface coatings [76]. With the improved first layer adhesion, sintered NaCl salt cores can be used in AFPisc. It depends on the part and process requirements whether the spray coating is sufficient or if pressure assisted coating is necessary. The spray coating is the most flexible method. It can cover undercuts, but produces just a thin layer with a weak adhesion. Its water content may cause porosity or salt degradation. The press coating ensures a constant and thicker coating with a good adhesion. However, it may cause cracks or deformation of fragile salt parts.

It has not been investigated yet, if another salt material is appropriate for such surface treatments, too. Other salt species or production methods might have different surface properties in terms of roughness, porosity and chemical reactivity, which may lead to different bonding options.

3 CONCLUSION

This study investigated the binder-free salt core technology for a selection of FRP processes with different boundary conditions, namely injection molding and AFPisc. The experiments show that there is potential to use binder-free conventional salt cores thanks to their higher strength, density, water-solubility, and recycling capability. Starting from this point, adaptions can to be made to ensure a robust processing. The main conclusions can be summarized as follows:

- Sintered salt cores can withstand an injection molding processes with neat PA6. A core thickness of 2 mm is feasible with the proposed method of a rib reinforcement combined with a filling strategy that reduces bending loads. However, those salt cores are not viable in CF-PEEK injection molding, because the salt strength drops severely as temperature rises. The low wall thickness of the core does not provide enough heating resistance to prevent the core center temperature exceeding a critical limit if it is placed in a preheated mold for PEEK.
- Salt cores made by HPDC with a minimum wall thickness of 20 mm seem to have potential in CF-PEEK injections. A flawless salt part withstands the process loads. This leads to a to a high salt-to-PEEK ratio of 8:1 for the proposed geometry [69]. The bulky design causes tolerance issues and large porosities in the salt core that lead to scrap parts. Adaptions will be necessary to achieve a reliable process. A reworked mold design for the salt core casting will probably provide sound core segments.
- The strength drop of the salt at processing temperatures for PEEK requires high wall thickness and hinders a preheating of the core to mold temperature.
- The salt cores are washed out in a water bath. Complete dissolution is achieved. A pressured water jet shortens the core removal time. Because the salt is not contaminated, it could be reused after the evaporation of water. Eventually, an additional milling process is needed to ensure the optimal gain size for sinter methods.
- The critical first layer adhesion for additive processes like CF-PEEK tape placement with AFPisc can be improved with PEEK spray or foil coating. The foil coating leads to superior interface properties. It leaves a robust, matrix-rich film on the surface, which increases the peel resistance of the tape. However, thin salt structures may be deformed by the residual stresses caused by the foil application and process control adaptions are necessary to improve the first layer adhesion for AFPisc.

The presented study shows, that binder-free salt cores can have a wide application field in plastics technology. The good thermomechanical properties combined with the water-solubility at low temperatures makes them an interesting alternative to common core materials based on waxes, low-melt alloys or sand

cores. Nevertheless, challenging process conditions as for CF-PEEK injection molding show the limits of the salt material. Furthermore, thermoplastic tapes with continuous Carbon fibers can be attached to a binder-free salt core which may result in a hybrid insert, i.e. a core that can be washed out with water, but supports fragile tape laminates during the overmolding.

4 OUTLOOK

Conventional, binder-free salt cores offer new possibilities for plastics manufacturing processes and encourage further research on the topic. However, the thermomechanical behavior of the various salts should be characterized in dedicated experiments so that there is a database for filling simulations, which will then be able to forecast core deformation or damage during an injection molding operation. A suitable filling strategy must be found for cast salt cores with a high variance in thickness. In order to make use of their full potential, a deeper investigation of joining and machining operations should be considered. Perhaps surface treatments can improve the chemical affinity towards adhesives or coatings of the pure and thus rather inert salt. Alternatively, an assembly of salt segments through form closure can replace fragile material closure joints. However, in this case, a design must be chosen, that avoids tensile stress. In order to increase the geometric versatility of sintered or cast salt cores, an appropriate setup for cutting operations should be investigated, that accounts for the brittleness of the material. Furthermore, such salt cores may be worth to be tested in resin infusion or sheet molding compound processes, too. Their density and strength will likely outperform other expendable core materials in those applications.

The tensile sensitivity and brittle failure behavior are major drawbacks of unreinforced, binder-free salt cores that limit their application. Therefore, the authors will suggest fiber reinforcements for salt cores that increase the key features bending strength and energy absorption in a follow-up paper.

5 ACKNOWLEDGEMENT

The authors would like to thank the European Commission for the funding of the project IMCoLoR (partners: apppex GmbH, FACC, TPRC, TUM; grant agreement ID: 738131) in the framework of Horizon 2020 - Clean Sky 2. Furthermore, we appreciate the funding from BMWi for the ZIM cooperation project Slokav (partners: apppex GmbH, TUM; grant code: ZF4004305EB5). We are grateful to FH Wels, Upper Austria, for the CT scans and all students, technicians and colleagues who contributed to the project work. In addition, we are grateful for the kind support from the companies KraussMaffei Technologies GmbH and TenCate Advanced Composites (now: Toray Advanced Composites).

6 GLOSSARY

ABS acrylonitrile butadiene styrene
AFP automated fiber placement
CA cyanoacrylate adhesive
CF carbon fiber
CFRP carbon fiber reinforced plastic
CT computer tomography
CTE coefficient of thermal expansion
DC dispersion coating
FC foil coating
FRP fiber-reinforced plastic
GC gravity casting
HP hot press process
HPDC high pressure die-casting
IR infrared
isc in-situ consolidation
LEF layered extrusion forming
LPDC low pressure die-casting
P press process
PA polyamide
PAEK polyaryletherketone
p_c consolidation pressure
PEEK polyetheretherketone
PP polypropylene
PS poylstyrene
RTM resin transfer molding
S sintering process
T temperature
WCM wet compression molding

REFERENCES

[1]	Johannaber, F.; Michaeli, W.	Handbuch Spritzgießen 2nd ed., Hanser, München, 2004 DOI: 10.3139/9783446440982
[2]	Erhard, G.	Konstruieren mit Kunststoffen 4th ed., Hanser, München, 2008
[3]	Hauck, C.; Schneiders, A.	Optimieren der Schmelzkerntechnik für das Thermoplast-Spritzgießen Kunststoffe 77 (1987) 12, pp. 1237–1240
[4]	Lin, K.-Y.; Chang, F.-A.; Liu, S.-J.	Using differential mold temperatures to improve the residual wall thickness uniformity around curved sections of fluid assisted injection molded tubes International Communications in Heat and Mass Transfer 36 (2009) 5, pp. 491–497 DOI: 10.1016/j.icheatmasstransfer.2009.02.009
[5]	Parvez, M. A.; Ong, N. S.; Lam, Y. C. et al.	Gas-assisted injection molding: the effects of process variables and gas channel geometry Journal of Materials Processing Technology 121 (2002) 1, pp. 27–35 DOI: 10.1016/S0924-0136(01)01184-0
[6]	Grözinger, H. D.	Wasserlöslicher Salzkern mit Funktionsbauteil DE 10 2006 031 532 B3 07 July 2006
[7]	Wüst, A.	Herstellung von hohlen Formkörpern im Kernschmelzverfahren und hierbei verwendete Hohlkörpergeometrie DE 195 15 974 A1 02 May 1995
[8]	Wintermantel, E.; Ha, S.-W. (Eds.)	Medizintechnik 4th ed., Springer, 2008 DOI: 10.1007/978-3-540-74925-7

[9]	Brandwijk, R.	Manufacturing and optimization of a PEEK scroll by fusible core injection moulding - Final Report Summary Project 632445 (THERMOPLASTIC SCROLL), Clean Sky, 2016 Available [Accessed 31.06.2022]: https://cordis.europa.eu/project/id/632445/reporting
[10]	N.N.	Weniger ist jetzt noch mehr - Pumpengehäuse aus kohlenstofffaserverstärktem PEEK 15 June 2015 Available [Accessed 30 June 2022]: https://www.kunststoffe.de/a/produktmeldung/weniger-ist-jetzt-noch-mehr-247830#
[11]	N. N.	The Lowdown on Lost Cores 03 June 1998 Available [Accessed 05 August 2021]: https://www.plasticstoday.com/lowdown-lost-cores
[12]	Grözinger, H. D.	Verwendung von Salzkernen für Kunststoffguss und Verfahren zur Herstellung von Kunststoff-Hohlformkörpern EP2040897B1 09 July 2007
[13]	Xiao, Z.; Harper, L. T.; Kennedy, A. R. et al.	A water-soluble core material for manufacturing hollow composite sections Composite Structures 182 (2017), pp. 380–390 DOI: 10.1016/j.compstruct.2017.09.058
[14]	Thiede-Smet, M.; Wadsworth, M.	Tooling inserts for resin transfer moulding In: Kruckenberg, T. M.; Paton, R. (Eds.) Resin Transfer Moulding for Aerospace Structures, 1st ed. Springer Dordrecht, Netherlands, 1998, pp. 338–387 DOI: 10.1007/978-94-011-4437-7

[15] Keller, C. W.
Fiberglass supports for cryogenic tanks
NASA, Lockheed Missiles and Space Co. Sunnyvale, CA, United States, 1972
Available [Accessed 12 August 2021]:
https://ntrs.nasa.gov/citations/19720025914

[16] Lin, C.-C.; Yang, C.-L.
A Water-Soluble Core for Manufacturing Hollow Injection-Molded Products
Polymers 14 (2022) 11, pp. 1–15
DOI: 10.3390/polym14112185

[17] Campbell, J.
Complete casting handbook
2nd ed., Butterworth-Heinemann, Amsterdam, 2015

[18] Hartig, T.; Schiller, G.; Bütterich, C.
Salt Core Technology. Lost cores aluminium casting applications
Emil Müller GmbH, Wilhermsdorf, 2018

[19] Kugel, A.; Bührig-Polaczek, A.
Möglichkeiten zur Erzeugung von Hohlräumen in Druckgussteilen
Gießereiforschung 56 (2004) 1, pp. 14–22

[20] Yaokawa, J.; Miura, D.; Anzai, K. et al.
Strength of Salt Core Composed of Alkali Carbonate and Alkali Chloride Mixtures Made by Casting Technique
Materials Transactions 48 (2007) 5, pp. 1034–1041
DOI: 10.2320/matertrans.48.1034

[21] Czerwinski, F.; Mir, M.; Kasprzak, W.
Application of cores and binders in metalcasting
International Journal of Cast Metals Research 28 (2015) 3, pp. 129–139
DOI: 10.1179/1743133614Y.0000000140

[22] Fuchs, B.
Salzkerntechnologie für Hohlgussbauteile im Druckguss
1st ed., Audi Dissertationsreihe, Vol. 96, Cuvillier Verlag, Göttingen, 2014

[23] Kallien, L. H.
Salzkerne im Druckguss
Giesserei-Special (2016) 01, pp. 32–43

[24]	Fickel, P.	Hohl- und Verbundguss von Druckgussbauteilen - Numerische Auslegungsmethoden und experimentelle Verifikation Dissertation, Universität Stuttgart, 2017 DOI: 10.18419/opus-9068
[25]	Herrmann, C.; Pries, H.; Hartmann, G. (Eds.)	Energie- und ressourceneffiziente Produktion von Aluminiumdruckguss 1st ed., Springer Vieweg, Berlin, Heidelberg, 2013 DOI: 10.1007/978-3-642-39853-7
[26]	Scheydecker, M.; Weisskopf, K.-L.	Innovationspotenzial Salzkerne. Herausforderungen für die Serienanwendung im Aluminium-Guss VDI-Berichte, Vol. 2217, Daimler AG, Ulm, 2014
[27]	Vollrath, K.	Herstellung hochwertiger Salzkerne durch Warmkammer-Druckgießen Giesserei 104 (2017) 01, pp. 32–37
[28]	Nitschke-Pagel, T.	Thermisches Fügen In: Henning, F.; Moeller, E. (Eds.) Handbuch Leichtbau. Methoden, Werkstoffe, Fertigung. Hanser, München Wien, 2011, pp. 855–885
[29]	Kallien, L. H.; Görgrün, V.	Einfluss der Elektromobilität auf die Gussproduktion in der deutschen Gießerei-Industrie Giesserei 105 (2018) 4, pp. 70–80
[30]	Kallien, L. H.; Görgrün, V.	Einfluss der Elektromobilität auf die Gussproduktion in der deutschen Gießerei-Industrie Giesserei 105 (2018) 7, pp. 60–66
[31]	Mählmann, H.; Baader, M.	GDA Jahresbericht 2020 Gesamtverband der Aluminiumindustrie e.V., 2020 Available [Accessed 30 June 2022]: http://www.aluinfo.de/downloads-jahresberichte.html

[32] Wappelhorst, M.; Grov, N.
Schweiß- und wärmebehandelbarer Druckguss
Konstruieren und Giessen 32 (2007) 3, pp. 22–28

[33] Bonollo, F.; Gramegna, N.; Timelli, G.
High-Pressure Die-Casting: Contradictions and Challenges
The Minerals, Metals & Materials Society 67 (2015) 5, pp. 901–908
DOI: 10.1007/s11837-015-1333-8

[34] Murray, M. T.; Murray, M.
High pressure die casting of aluminium and its alloys
In: Lumley, R. (Ed.) Fundamentals of aluminium metallurgy. Production, processing and applications, 1st ed. Woodhead Publishing Limited, Cambridge, 2011, pp. 217–261

[35] Long, A.; Thornhill, D.; Armstrong, C. et al.
Predicting die life from die temperature for high pressure dies casting aluminium alloy
Applied Thermal Engineering 44 (2012), pp. 100–107
DOI: 10.1016/j.applthermaleng.2012.03.045

[36] Gong, X.; Liu, X.; Chen, Z. et al.
3D Printing of High-Strength Water-Soluble Salt Cores via Layered Extrusion Forming (preprint)
The International Journal of Advanced Manufacturing Technology , In Review (2021)
DOI: 10.21203/rs.3.rs-546973/v1

[37] Jelínek, P.; Adámková, E.; Mikšovský, F. et al.
Advances in Technology of Soluble Cores for Die Castings
Archives of Foundry Engineering 15 (2015) 2, pp. 29–34
DOI: 10.1515/afe-2015-0032

[38] Jiang, W.; Dong, J.; Lou, L. et al.
Preparation and Properties of a Novel Water Soluble Core Material
Journal of Materials Science & Technology 26 (2010) 3, pp. 270–275

[39] Dworog, A.
Abschlussbericht des Verbundprojektes 3D-Freiformkanäle im Druckguss / Medienführende Kanäle
BMBF Forschung für die Produktion von morgen, Förderkennzeichen 02PU2243, Nordwalde, 2011

[40] Kaerger, J. C.; Atz, L.
Water Soluble Mandrels for Lost Core Applications in Manufacturing of Hollow Composite Structures
SAMPE Journal 57 (2021) 4, pp. 8–17

[41] Oikawa, K.; Meguro, K.; Yaokawa, J. et al.
Mechanical Properties of Mixed Salt Core Made by Die Casting Machine
Journal of Japan Foundry Engineering Society 81 (2009) 5, pp. 232–237
DOI: 10.11279/jfes.81.232

[42] Pierri, D.; Beck, C.
Lost Core Technologie - offen für alle. Chancen und Grundlagen des Verfahrens
Giesserei 103 (2016) 10, pp. 46–52

[43] Kallien, L. H.; Weidler, T.; Becker, M.
Production of magnesium die castings with hollow structures using gas injection technology in the hot chamber die casting process
International Foundry Research 66 (2014) 4, pp. 20–27

[44] Kallien, L. H.; Böhnlein, C.; Dworog, A. et al.
Ergebnisse aus dem Forschungsprojekt 3-D-Freiform – medienführende Kanäle im Druckguss
Giesserei 100 (2013) 12, pp. 36–43

[45] Huang, R.; Zhang, B.
Study on the Composition and Properties of Salt Cores for Zinc Alloy Die Casting
International Journal of Metalcasting 11 (2017) 3, pp. 440–447
DOI: 10.1007/s40962-016-0086-7

[46] Grözinger, H. D.
Salt Cores for Plastic (Injection) Molding
US8017056B2
13 September 2011

[47] Grözinger, H. D.
Wasserlösliche Salzkerne für den Druckguss
WO 2005/080022 A2
17 February 2005

[48] Oikawa, K.; Sakakibara, K.; Yamada, Y. et al.
High-Temperature Mechanical Properties of NaCl–Na2CO3 Salt-Mixture Removable Cores for Aluminum Die-Casting
Materials Transactions 60 (2019) 1, pp. 19–24
DOI: 10.2320/matertrans.MG201804

[49] Vitor, P. A. M.; Santos, P. H. F.; Alves, A. K. et al.
Study of Densification by Pressing and Sintering of NaCl and KCl Salts
7th International Congress on Ceramics & 62º Congresso Brasileiro de Cerâmica (2018), pp. 734–740

[50] Tu, S.; Liu, F.; Li, G. et al.
Fabrication and characterization of high-strength water-soluble composite salt core for zinc alloy die castings
The International Journal of Advanced Manufacturing Technology 95 (2018), pp. 505–512
DOI: 10.1007/s00170-017-1208-y

[51] Findeisen, S.; van der Auwera, R.; Heuser, M. et al.
Gießtechnische Herstellung von E-Motorengehäusen mit interner Kühlung
Giesserei 106 (2019) 06, pp. 72–78

[52] Gong, X.; Jiang, W.; Liu, F. et al.
Effects of glass fiber size and content on microstructures and properties of KNO3-based water-soluble salt core for high pressure die casting
International Journal of Metalcasting (2020)
DOI: 10.1007/s40962-020-00480-9

[53] Cantas, C.; Baksan, B.
Effects of Composition on the Physical Properties of Water-Soluble Salt Cores
International Journal of Metalcasting (2020)
DOI: 10.1007/s40962-020-00511-5

[54] Liu, F.; Tu, S.; Gong, X. et al.
Comparative study on performance and microstructure of composite water-soluble salt core material for manufacturing hollow zinc alloy castings
Materials Chemistry and Physics 252 (2020) 123257, pp. 1–10
DOI: 10.1016/j.matchemphys.2020.123257

[55] Wang, X.; Liu, W.; Liu, X. et al.
First-Principles Calculation and Mechanical Properties of NaCl–Na2SO4 Composite Water-Soluble Salt Core
International Journal of Metalcasting (2022)
DOI: 10.1007/s40962-022-00769-x

[56]	Telle, R. (Ed.)	Keramik 7th ed., Springer, Berlin Heidelberg, 2007
[57]	Goodall, R.; Despois, J.-F.; Mortensen, A.	Sintering of NaCl powder: Mechanisms and first stage kinetics Journal of the European Ceramic Society 26 (2006) 16, pp. 3487–3497 DOI: 10.1016/j.jeurceramsoc.2005.12.020
[58]	Schulze, D.	Pulver und Schüttgüter. Fließeigenschaften und Handhabung 4th ed., VDI-Buch, Springer, Berlin, Heidelberg, 2019 DOI: 10.1007/978-3-662-58776-8
[59]	Riedel, R.; Chen, I.-W. (Eds.)	Synthesis and Processing 1st ed., Ceramics Science and Technology, Vol. 3, Wiley-VCH Verlag GmbH & Co. KGaA, Weinheim, 2012 DOI: 10.1002/9783527631957
[60]	Kallien, L. H.; Böhnlein, C.	Verfahren zur Herstellung hohler Salzkerne DE102012108079B3 31 August 2012
[61]	Alwekar, S.; Ogle, R.; Kim, S. et al.	Manufacturing and characterization of continuous fiber-reinforced thermoplastic tape overmolded long fiber thermoplastic Composites Part B: Engineering 207 (2021) DOI: 10.1016/j.compositesb.2020.108597
[62]	Green, S.; Ferfecki, F. J.; Marburger, U.	Overmoulding of PEEK Compounds for Composites Aerospace Brackets SAMPE Journal 54 (2018) 3, pp. 20–27
[63]	Arquier, R.; Iliopoulos, I.; Régnier, G. et al.	Consolidation of continuous-carbon-fiber-reinforced PAEK composites: a review Materials Today Communications 32 (2022) Article 104036 DOI: 10.1016/j.mtcomm.2022.104036
[64]	Feldman, S. R.	Sodium Chloride, chapter Sodium Chloride Wiley-Interscience, 2005

[65]	Picard, P.	Complete Injection Overmolding of Local Unidirectional Carbon Fiber Reinforcements expoAir 2017, München, 2017
[66]	Elgeti, K.; Hahne, E.; Martin, E.	Wärmeleitung 10th ed., VDI-Wärmeatlas, Springer, Berlin, Heidelberg, 2002
[67]	Ullrich, M.	Experimentelle und simulative Untersuchung eines Spritzgussprozesses mit TP-AFP-Einlegern in Moldflow mit PA6 & PEEK Master Thesis, LCC, Technische Universität München, 2018
[68]	Wu, S.	Untersuchung von Integrationsmöglichkeiten verlorener Kernwerkstoffe in Composite-Fertigungsverfahren unter Berücksichtigung von Spritzguss und AFP-TPisc-Prozess Term Project, LCC, Technische Universität München, 2018
[69]	N. N.	Periodic Reporting for period 2 - IMCoLoR (Injection Moulding with Continuous Local Reinforcements) Project 738131(IMCoLoR), Horizon 2020, Clean Sky 2, 2020 Available [Accessed 31 May 2021]: https://cordis.europa.eu/project/id/738131/reporting
[70]	N. N.	Toray Cetex TC1225 LMPAEK Product Data Sheet Toray Advanced Composites, USA, The Netherlands, 2020 Available [Accessed 30 September 2022]: https://www.toraytac.com/product-explorer/products/gXuK/Toray-Cetex-TC1225
[71]	Haseli, P.; Jacob, R.; Liu, M. et al.	Experimental phase diagram study of the binary KCl-Na2CO3 system Thermochimica Acta 695 (2021) Article 178811 DOI: 10.1016/j.tca.2020.178811

[72]	Wettemann, T.	In situ manufactured carbon-thermoplastic curved stiffened panel - Deliverable No.:1.2 Final Report Project 686894 (INSCAPE), Horizon 2020, Clean Sky 2, 2018 Available [Accessed 31 August 2021]: https://cordis.europa.eu/project/id/686894/results
[73]	Kollmannsberger, A.	Heating characteristics of fixed focus laser assisted Thermoplastic-Automated Fiber Placement of 2D and 3D parts Dissertation, Technische Universität München, 2019
[74]	N. N.	APTIV® 1000 Series Films for Electrical Insulation Victrex plc, UK Available [Accessed 05 October 2022]: www.aptivfilms.com
[75]	N. N.	VICOTE® F804 Aqueous Dispersion for use on Ferrous Metals. 800 Series Aqueous Dispersions Product Data Sheet Victrex plc, UK Available [Accessed 28 June 2018]: www.vicote.com
[76]	Wu, S.	Entwicklung eines Beschichtungsverfahrens für Salzkerne in der Composite-Fertigung mit PAEK/PEEK-Matrix Master Thesis, LCC, Technische Universität München, 2019
[77]	Clancy, G.; Peeters, D.; O'Higgins, R. M. et al.	In-line variable spreading of carbon fibre/thermoplastic pre-preg tapes for application in automatic tape placement Materials & Design 194 (2020) Article 108967 DOI: 10.1016/j.matdes.2020.108967
[78]	Buchmann, C.; Langer, S.; Filsinger, J. et al.	Analysis of the removal of peel ply from CFRP surfaces Composites Part B: Engineering 89 (2016), pp. 352–361 DOI: 10.1016/j.compositesb.2015.11.019

[79] Stokes-Griffin, C. M.; Compston, P.
A combined optical-thermal model for near-infrared laser heating of thermoplastic composites in an automated tape placement process
Composites Part A: Applied Science and Manufacturing 75 (2015), pp. 104–115
DOI: 10.1016/j.compositesa.2014.08.006

[80] Bharath Sabarish, V. C.; Durairajan, A.; Gajendiran, J. et al.
Preparation of low cost NaCl single crystal for IR optical window applications
Journal of Materials Science: Materials in Electronics 32 (2021) 20, pp. 24971–24979
DOI: 10.1007/s10854-021-06955-7

Keywords:
salt core**,** expendable core, removable core, water-soluble core, wash-out mandrel, lost core, semi-permanent mold, binder-free salt, NaCl, overmolding, injection molding, PA6, PEEK, first layer adhesion, AFP, tape placement, in-situ consolidation, additive manufacturing

Stichworte:
Salzkern, verlorener Kern, entfernbarer Kern, wasserlöslicher Kern, auswaschbarer Kern, temporäre Form, binderloses Salz, NaCl, Umspritzen, Spritzguss, PA6, PEEK, Erstlagenanbindung, AFP, Tapelegen, in-situ Konsolidierung, additive Fertigung

Autoren / authors:
M. Sc. Dominik Boos
Dr.-Ing. Swen Zaremba
Prof. Dr.-Ing. Klaus Drechsler
Chair of Carbon Composites
Technical University of Munich
Boltzmannstraße 15
85748 Garching bei München

E-Mail: zaremba@tum.de
Homepage: www.asg.ed.tum.de/en/lcc
Phone: +49 (0)89 289 15081
Fax: +49 (0)89 289 15097

M. Sc. Tim Scherzer
University of Bayreuth
Department of Polymer Engineering
Universitätsstraße 30, FAN A
95447 Bayreuth